

# Atomistic Calculations of the Effect of Minor Actinides on Thermodynamic and Kinetic Properties of $UO_{2\pm x}$

---

## Integrated University Programs

Dr. Chaitanya Deo  
Georgia Institute of Technology

In collaboration with:  
Los Alamos National Laboratory  
Sandia National Laboratory

Cetin Unal, Technical POC  
Frank Goldner, Federal POC

# NEUP Final Report

---

## Atomistic calculations of the effect of minor actinides on $\text{UO}_{2\pm x}$

**PI: Dr. Chaitanya Deo, Assistant Professor, Georgia Institute of Technology**

**Proposal ID: 09-823**

**Tracking ID: CFP-09-267**

### Table of Contents

Atomistic calculations of the effect of minor actinides on $\text{UO}_{2\pm x}$ .....	1
Introduction .....	2
Project Objective.....	2
Work Performed and results.....	3
Publications and presentations.....	3
Publications:.....	3
Presentations .....	4
Future Outlook of the research and development.....	5
Appendices:.....	7
Results and work done are presented in the attached Appendices.....	7

## Introduction

The chemistry of nuclear reactor fuel initially is complex, and continuous loss of uranium and plutonium and formation of a broad range of new species due to fission introduce a challenging time-dependence to this chemistry. The fuel ultimately contains multiple f-electron elements: uranium, plutonium, americium, neptunium, and curium as well as many lighter elements. This situation leads to the potential formation of many phases that can influence critical physical properties. In order to understand the microstructural evolution of nuclear fuels during operation and fabrication, one must first understand the thermodynamic driving forces driving these microstructural changes as well as kinetic parameters that determine how quickly these changes occur.

We examined how the incorporation of other actinide species, important for MOX and other advanced fuel designs, impacts thermodynamic quantities of the host  $\text{UO}_2$  nuclear fuel and how Pu, Np, Cm and Am influence oxygen mobility. In many cases, the experimental data is either insufficient or missing. We employed atomistic modeling tools to calculate these quantities.

During burn-up, oxide nuclear fuel exhibits very significant restructurings of the microstructure, including the formation of metal precipitates, porosity, grain boundary evolution, and phase segregation. This evolution of the material is the result of mass redistribution in the fuel, and is even more pronounced in fast reactors. Unlike conventional light water reactor fuels, the presence of minor actinides increases the complexity of the microstructural evolution and consequently, analysis of the structure property relationships.

These minor actinides influence the properties of the fuel by changing the structure of the host matrix ( $\text{UO}_2$ ,  $\text{PuO}_2$  or MOX). New phases may form, localized to the vicinity of high species concentration. For many of these multicomponent systems that involve concentrations of minor actinides in the host oxide matrix, thermodynamic quantities and phase stabilities are rarely available.

## Project Objective

The main objective of the project was to understand the nature of actinide incorporation in oxide fuel matrix. Minor actinides such as Th, Pu, Np, Am were considered.

The project looked at the effect of minor actinide substitution on  $\text{UO}_2$  lattice as well as the structure of (Th, U)  $\text{O}_2$  fuel. Fundamental physical properties such as elastic constants, moduli, phonon dispersion curves and defect formation energies were computed. Oxygen mobility in the case of non-stoichiometric  $\text{UO}_2$  was calculated as well.

Some unique challenges were encountered. These included the use of DFT+U -based first principles techniques for calculating some actinide properties. These were found to be very unreliable for some actinide oxides. Thus recourse was taken to empirical molecular statics calculations to determine these quantities.

## Work Performed and results

Work performed is described in the appendices and well documented in the publications and presentations listed below.

Appendix 1: Incorporation of lanthanides and minor actinides in UO<sub>2</sub>

Appendix 2: Development of interatomic potentials capable of simulating mixed (U,Th)O<sub>2</sub>

## Publications and presentations

The project resulted in 6 publications as well as 8 presentations at conferences. These are:

### Publications:

JA1;JA2;PR3;TR4;JA5;JA6

JA1 R. Behera, and C. Deo. 2012. Atomistic Models to Investigate Thorium Dioxide (ThO<sub>2</sub>). *Journal of Physics-Condensed Matter* 24 (21):215405.

JA2 R. Behera, C. Deo, and H. Xu. 2012. Effect of the substitution of f-electron elements on the structure and elastic properties of UO<sub>2</sub>. *Journal of Nuclear Materials* accepted for publication August 2012

PR3 Rakesh K. Behera, and Chaitanya S. Deo. 2012. Effect of Ce<sup>4+</sup> and Th<sup>4+</sup> Ion Substitution in Uranium Dioxide. MRS Proceedings Library, doi:10.1557/opl.2012.240

TR4 R. Behera, and C. Deo. 2011. Development of Interatomic Potentials to Investigate ThO<sub>2</sub>-Based Mixed Oxide Fuels. Transactions of the American Nuclear Society Annual Meeting,

JA5 D. A. Andersson, J. Lezama, B. P. Uberuaga, C. Deo, and S. D. Conradson. 2009. Cooperativity among defect sites in  $\text{AO}(2+x)$  and  $\text{A}(4)\text{O}(9)$  ( $\text{A}=\text{U},\text{Np},\text{Pu}$ ): Density functional calculations. *Physical Review B* 79 (2):024110.

JA6 D. A. Andersson, T. Watanabe, C. Deo, and B. P. Uberuaga. 2009. Role of di-interstitial clusters in oxygen transport in  $\text{UO}(2+x)$  from first principles. *Physical Review B* 80 (6)

### Presentations

CP1;CP2;CP3;CP4;CP5;CP6;CP7;CP8

CP1 **R. Behera**, and C. Deo. 2011. Characterization of  $\text{ThO}_2\text{-UO}_2$  Mixed Oxide System Using Atomic Level Simulations. Materials Science and Technology MS&T 11: Symposium on Materials Science Challenges for Nuclear Applications, October 16-20, 2011,

CP2 **R. Behera**, and C. Deo. 2011. Investigation of  $\text{ThO}_2$ -based Mixed Oxide Fuels Using Atomic Level Simulations. International Conference on Emerging Nuclear Energy Systems, Symposium on Modeling and Simulation, May 15-19, 2011, San Francisco, CA.

CP3 **R. Behera**, and C. Deo. 2011. Atomistic Properties of  $\text{ThO}_2$  Based Nuclear Fuels. MRS Spring 2011, Symposium RR: Fundamental Science of Defects and Microstructure in Advanced Materials for Energy, April 25-29, 2011, San Francisco, CA.

CP4 **R. Behera**, and C. Deo. 2011. Development of Interatomic Potentials to Investigate  $\text{ThO}_2$ -Based Mixed Oxide Fuels. American Nuclear Society Annual Meeting, MSTD Symposium on Nuclear Fuels and Materials, June 26-30, 2011, Hollywood, FL.

CP5 **R. Behera**, C. Deo, D. Andersson, B. Uberuaga, and T. Watanabe. 2011. Effect of Stoichiometry and Temperature on the O/M Ratio in  $\text{UO}_{2+x}$ . MRS Spring 2011, Symposium RR: Fundamental Science of Defects and Microstructure in Advanced Materials for Energy, April 25-29, 2011, San Francisco, CA.

CP6 **A. Lord**, C. Deo, and D. Andersson. 2011. First principles calculations of elastic constants of mixed oxide (U, Pu)O<sub>2</sub> nuclear fuels. American Nuclear Society Student Conference, April 14-17, 2011, Atlanta, GA.

CP7 C. Deo. 2010. Multiscale modeling of Nuclear Fuel Materials INVITED. International Conference on Computational and Experimental Engineering and Sciences Special Symposium on Advanced Materials, March 28-April 1, 2010, Las Vegas, NV.

CP8 ———. 2009. Modeling and Simulation of Defect Mechanics in Nuclear Materials **INVITED**. Materials Science and Technology (MS&T), Symposium: Microstructure Characterization, Analyses, and Design, October 25-29, 2009, Pittsburgh, PA.

## Future Outlook of the research and development

The question of dealing with minor actinides is an important one. Reprocessing fuel requires an understanding of how these elements redistribute and interact with the host lattice. The present work is a start at developing atomistic information about these interactions. In order to understand the microstructural evolution of nuclear fuels during operation and fabrication, one must first understand the thermodynamic driving forces driving these microstructural changes as well as kinetic parameters that determine how quickly these changes occur.

Future work may proceed along following lines:

1. The present results may be linked thermodynamic models such as CALPHAD and obtaining the phase diagrams of these minor actinides with Uranium compounds. Thus, using the calculations of fundamental quantities - elastic constants, moduli, phonon dispersion - atomistic free energies will be calculated.
2. The present results may be coupled with microstructural models for simulating microstructural evolution of these fuels containing minor actinides as a function of operation and fabrication (sintering). This may involve studying the segregation of these minor actinides to grain boundaries, dislocations and microstructural features in these reprocessing fuels.

3. Combine high resolution 3D discrete ordinates burnup calculations with materials modeling methods developed here in order to obtain an understanding of how fission products in **minor actinide containing nuclear fuel** are formed and migrate in fuel during burnup. The emphasis will be on determining the hyper-accurate generation and evolution of minor actinides and fission products in fuel as it in a (presumable fast) reactor. Burnup calculations will be connected to atomistic molecular calculations of properties, as well as kinetic rate theory and microstructural models of fuel behavior for an nominal oxide fuel pin in a light water reactor and a metallic fuel pin in a fast reactor configuration.

4. The results here may be used to develop a better understanding of the thorium fuel cycle. Thorium oxide is a more stable oxide than UO<sub>2</sub> and its performance under irradiation is expected to be better than UO<sub>2</sub>. Some possibilities are to determine the thermal conductivity of mixed (Th,U)O<sub>2</sub> fuel as a function of composition and compare to the thermal conductivity of the pure ThO<sub>2</sub> and pure UO<sub>2</sub> at the atomistic scale, to determine the diffusivity of intrinsic point defects (vacancies, interstitials and clusters) and the oxygen-metal (O/M) ratio in the mixed oxide fuel with the atomistic methods and to Understand the fundamental mechanisms of the formation, diffusion and aggregation of fission gases (Xe and Kr) in the mixed (Th,U)O<sub>2</sub> fuel including their interaction with intrinsic point defects and grain boundaries.

**Appendices:**

**Results and work done are presented in the attached Appendices**

## Appendix 1

### **Effect of the substitution of f-electron elements on the structure and elastic properties of UO<sub>2</sub>**

In this study we have investigated the structural and mechanical properties of UO<sub>2</sub> and substituted urania-systems using atomic level simulations. While the qualitative trends predicted with molecular dynamics (MD) simulation is very useful, the quantitative comparison with experiment depends on the fidelity of the interatomic potentials used to describe the system. Since we are interested in characterizing the structural and elastic properties of UO<sub>2</sub> and substitution of Lanthanides and Actinides in the urania matrix, we have collected potentials which are consistent and transferable.

The ground state phase of UO<sub>2</sub> exhibits the Fluorite structure with  $Fm\bar{3}m$  symmetry (space group # 225). In the UO<sub>2</sub> lattice, uranium ions occupy the face centered positions and oxygen ions occupy the tetrahedral sites. In order to simulate urania systems with Lanthanides and Actinides, we have collected a set of interatomic potentials Article4;7;8;10;14;17;18. We have selected potentials where the O-O interactions are the same and transferable between U and other elements of interest. A list of self-consistent interatomic potentials available to describe the Lanthanides and Actinides are listed in Table 1. These potentials can be separated based on the charge definition on each ion. The potentials can be defined as a shell-model or rigid-ion model. In the shell model 21, each ion is described by a core and a shell, the sum of whose charges is the ionic charge of each species. The core and shell on each ion is attached to each other via a spring (which can be harmonic or anharmonic). The interaction between the core and shell of an atom coupled by a harmonic spring is given by:

$$V(\omega) = \frac{1}{2}k_2\omega^2 \quad (1)$$

where  $\omega$  is the core-shell displacement, and  $k_2$  is the harmonic spring constants. The interatomic potentials with shell-model are Grimes01 18, Grimes02 17, Grimes03 8 and Nadeem 14 referred as Pot1, Pot2, Pot3 and Pot4 respectively from hereinafter. Pot1 can describe U<sup>4+</sup>, and Ce<sup>4+</sup>, while Pot2 provides consistent parameters for U<sup>4+</sup>, Pu<sup>4+</sup>, Ce<sup>4+</sup>, Ce<sup>3+</sup>, Sm<sup>3+</sup>, and Gd<sup>3+</sup>. Pot3 is the only potential that can describe the most 3+ ion descriptions and includes consistent parameters to describe U<sup>4+</sup>, U<sup>3+</sup>, Pu<sup>4+</sup>, Pu<sup>3+</sup>, Nd<sup>3+</sup>, Sm<sup>3+</sup>, Eu<sup>3+</sup>, and Gd<sup>3+</sup>. Pot4 can describe systems with Th<sup>4+</sup>, U<sup>4+</sup>, and Ce<sup>4+</sup>. There are two rigid ion models, where the ions are defined by point charges. The Osaka potential (Pot5) 7 can describe most of the Actinides (Th<sup>4+</sup>, U<sup>4+</sup>, Np<sup>4+</sup>, Pu<sup>4+</sup>, and Am<sup>4+</sup>) and Gd<sup>3+</sup> consistently; while Uchida potential (Pot6) Article4;10 has self-consistent parameters to describe a few Actinides (Th<sup>4+</sup>, U<sup>4+</sup>, Am<sup>4+</sup>, and Am<sup>3+</sup>) of

interest.

In order to simulate the urania systems with lattice-statics and MD approach, the overall interactions are defined by the sum of long-range and short-range contributions. The long-range interactions for all the potentials are described by the Coulombic interaction.

$$V_{Coul}(r_{ij}) = \frac{1}{2} \sum_{i=1}^N \left\{ \sum_{j \neq i} \frac{q_i q_j}{r_{ij}} \right\} \quad (2)$$

where  $N$  is the total number of ions in the system,  $q_i$ ,  $q_j$  are the magnitude of charges on ions  $i$  and  $j$ , and  $r_{ij}$  is the separation between ions  $i$  and  $j$ . The Ewald sum approach is used to estimate the Columbic interactions within a finite cut-off distance.

The short-range interactions are described predominantly by strong repulsive interactions. All the potentials considered in this article describes the short-range interaction by the Buckingham potential 22 form, which is given as:

$$V_{Buck}(r_{ij}) = A_{ij} \exp(-r_{ij}/\rho_{ij}) - C_{ij}/r_{ij}^6 \quad (3)$$

where  $r_{ij}$  is the separation between two ions  $i$  and  $j$ ; and  $A$ ,  $\rho$ , and  $C$  are free parameters. Pot5 and Pot6 includes an additional Morse potential 23, which is used to describe the covalent bonding in the system. The Morse potential is given as:

$$V_{Morse}(r_{ij}) = D_{ij} \left\{ \left[ 1 - \exp(-\beta_{ij}(r_{ij} - r_{ij}^*)) \right]^2 - 1 \right\} \quad (4)$$

where  $r_{ij}$  is the separation between two ions  $i$  and  $j$ ; and  $D$ ,  $\beta$  and  $r_{ij}^*$  are free parameters. All the potential parameters are given in Tables 2a and 2b.

The General Utility Lattice Program (GULP) 13;16 was used to predict the structural and elastic properties discussed in this article. The simulations were performed within a 30% substitution of the  $U^{4+}$  ions, which is in line with the concentration ranges reported in the literature for  $UO_2$  systems. In the input structures, the substituted ions were randomly distributed in the urania matrix for all the concentrations. Following the work by Xu *et al.* 3 on similar Fluorite system, a 4 x 4 x 4 supercell (768 atoms for bulk phases) was used to perform all the calculations.

The random distribution of substituted ions depends on the configurational space available in the input structure and thus on the size of the simulation supercell. There are different approximations that can be employed to establish solid solution configuration using smaller supercells. These methods are extremely attractive for first-principles calculation, which is limited by system size. The approximations are (i) coherent potential approximation (CPA), (ii) cluster expansion (CE), and (iii) special-quasirandom structure (SQS) Article2. While CPA and CE are useful for first-principles calculation, SQS method can be used for both first-principles and atomistic simulations. In the SQS method, structures are generated which mimics the correlation functions of an infinite random system within a finite supercell. For a

random alloying of Al-Ti system, von Pezold *et al.* Article2 reported that the SQS method with a  $2 \times 2 \times 2$  (32 atom) supercell resulted in similar elastic properties as a randomly distributed alloy system with  $4 \times 4 \times 4$  supercell containing 256 atoms. Since, all the calculations in this manuscript are performed with a  $4 \times 4 \times 4$  supercell containing 768 atoms, the random distribution of substituted ions are used to evaluate the structural and elastic properties.

For all the substituted ions, the relationship between the Shannon ionic radii  $r_0$  and the atomic number is presented in Figure 1. Figure 1(a) illustrates the ionic radii variation with atomic number for Lanthanides, while Figure 1(b) illustrates the variation for Actinides. In general, the ionic radii of 3+ ions are larger than 4+ ions, which is as expected. The ionic radius decreases with the increase in atomic number for a particular charge state. The ionic radii of 3+ ions are presented with two different coordination numbers (CN = 6 and 8). Since we are substituting 3+ ions in  $\text{UO}_2$ -matrix, we have considered the ionic radii with CN = 8 for discussion.

There are different mechanisms associated with 4+ and 3+ ion substitution. Substitution of 4+ ions at the cation sites of the urania matrix ( $\text{U}_{1-x}\text{A}_x\text{O}_2$ ) does not change the electrostatic of the system. Therefore, the change in lattice parameter due to 4+ ion substitution can be assigned to the change in the radii of the substituted ions, i.e. the elastic effect. A smaller ionic radius relative to  $\text{U}^{4+}$  ion will create local compression, thereby is expected to reduce the lattice parameter. Similarly, a larger ionic radius will create local tension, which will tend to increase the lattice parameter. On the other hand, we have to consider both elastic and electrostatic effects to understand the response of 3+ ions substitution in the urania matrix ( $\text{U}_{1-2x}\text{A}_{2x}\text{O}_{2-x}$ ). Xu *et al.* 3 have reported the possible effects of 3+ ions in a  $\text{CeO}_2$  matrix. Similar structural response is expected for 3+ ion substitution in  $\text{UO}_2$ . The electrostatic response for +3 ion substitution should increase the lattice parameter due to (i) the reduction in electrostatic attraction, (ii) increase in electrostatic repulsion due to the oxygen vacancies. The elastic response due to the substitution of a larger ionic radius ion (+3 ions have larger ionic radii than  $\text{U}^{4+}$  ion, see Figure 1) will increase the lattice parameter. However, the increase in the number of vacancies due to the increase in the +3 ions in the system reduces the density of the overall system. Hence, there are three factors acting towards increasing the lattice parameter, and one towards reducing the lattice parameter. The overall effect for different 4+ and 3+ ions are discussed in detail.

## 1. Results

### 3.1 Pristine $\text{UO}_2$

Each interatomic potential that we employ has been fit to pristine  $\text{UO}_2$  properties. The bulk properties of  $\text{UO}_2$  predicted from each potential are summarized in Table 3. These include the lattice parameter, elastic properties, dielectric constants and phonon properties. As seen from the table, most pristine, pure  $\text{UO}_2$  properties are well

predicted by these interatomic potentials. A detailed review is provided by Govers *et al.* 5;6. Except Pot4, all other potentials underestimated the lattice parameter. Pot1 underestimates the lattice parameter by ~0.15%, while Pot6 by ~0.45% compared to <0.1% by the rest of the potentials. Pot4 overestimates the lattice parameter by ~0.1%. Most of the potentials overestimated individual elastic constants. Pot5 predicts the  $C_{11}$  value within 10% of the experimental value, but it severely underestimates (~50%) the  $C_{12}$  value. All the potentials predict positive phonon frequencies, indicating the Fluorite structure to be stable.

We have calculated the anisotropy of the  $\text{UO}_2$  lattice as well as polycrystalline elastic moduli, which are not calculated before. The individual elastic constants are used to calculate the Zener anisotropy factor (Z) and the properties of polycrystalline  $\text{UO}_2$ . The Z factor describes the anisotropy in the cubic system. Using  $C_{11}$ ,  $C_{12}$ , and  $C_{44}$ , the only non-zero tensor quantities for a cubic system, Z can be defined as:

$$Z = \frac{2C_{44}}{C_{11} - C_{12}} \quad (5)$$

where,  $Z = 1$  indicates a perfectly isotropic system, and  $Z < 1$  indicates an anisotropic system. The Z value calculated from experimental elastic constants is 0.44 (data in Table 4) and 0.47 (reported by Berman and Belle 19). Thus,  $Z < 1$  indicates that the  $\text{UO}_2$  system is anisotropic and the elastic moduli values will be a maximum along the [100] or cube direction and a minimum along the [111] or octahedral direction. Therefore, the value of the elastic properties along the octahedral direction is expected to be 44% of the axial direction. The estimated Young's modulus along the [111] direction is reported in Table 3. Berman and Belle 19 reported the experimentally measured Young's modulus along [111] direction and it is ~52% of the axial directions. This value is slightly higher than the Z value calculated using elastic constants. Table 3 shows the values calculated for each  $\text{UO}_2$  potential using Equation 5. Except Pot5, all other potentials overestimated the Z value. Using Equation 5 the anisotropy factor is estimated to be 0.47 for Pot1, 0.59 for Pot2 and Pot3, 0.66 for Pot4, and 0.69 for Pot6. The Z value for Pot5 is estimated to be 0.30 mainly due to the severe underestimation of  $C_{12}$ .

Using the individual elastic constants, and the Voigt-Reuss-Hill (VRH) approximation, we calculated the polycrystalline elastic moduli. The VRH approximation gives a lower ( $G_R$ ) and upper bound ( $G_V$ ) for the shear modulus, and is given as 3;12:

$$G_R = \frac{5(C_{11} - C_{12}) \times C_{44}}{4C_{44} + 3(C_{11} - C_{12})} < G < G_V = \frac{C_{11} - C_{12} + 3C_{44}}{5} \quad (6)$$

Since the bulk modulus for the single and polycrystalline samples are exactly the same, the bulk and shear moduli values can be used to estimate the Young's modulus of polycrystalline  $\text{UO}_2$ , which is given as:

$$E_R = \frac{9B \times G_R}{(3B + G_R)} \quad , \quad E_v = \frac{9B \times G_v}{(3B + G_v)} \quad (7)$$

Table 3 lists the lower and upper bounds of Shear and Young's modulus calculated from experiment and empirical potentials.

After analyzing the structural and elastic properties of pure  $\text{UO}_2$ , we are interested in characterizing the variation of these due to the substitution of heavy ions. Since the lattice parameter changes due to substitution of 4+ and 3+ ions at a constant temperature, we have estimated the lattice parameter variation with a physical parameter defined as chemical expansion.

### 3.2 Chemical Expansion

Chemical substitution changes the lattice parameter and its effect can be analyzed by defining a chemical expansion analogous to the thermal expansion. While thermal expansion measures the variation in lattice parameter with change in temperature at constant pressure, chemical expansion measures the change in lattice parameter due to a change in chemical formula at constant temperature. Therefore, chemical expansion depends on the type of ions substituted in the host matrix (in this article it is urania matrix). While thermal expansion for most of the materials is positive with increase in temperature, the chemical expansion may be either positive or negative depending on the substituted ions (ion type, ionic radii, charge). Thus, we define the chemical expansion in  $\text{UO}_2$  as the change in lattice parameter due to substitution with respect to the lattice parameter of pure  $\text{UO}_2$ . The chemical expansion is defined as

$$\varepsilon_c = \left. \frac{(a - a_0)}{a_0} \right|_{T=\text{Constant}} \quad (8)$$

where  $a$  is the lattice parameter measured at any concentration, and  $a_0$  is the lattice parameter of  $\text{UO}_2$  perfect lattice. The measurements are performed at a constant temperature. The chemical expansion coefficient is generally defined as

$$\alpha_c = \frac{\varepsilon_c}{\Delta\delta} \quad (9)$$

where  $\Delta\delta$  is change in the oxygen-vacancy concentration in the system, and  $\delta$  is the measure of the oxygen-vacancy concentration.

However, since we are focusing on both +4 and +3 ion substitution in  $\text{UO}_2$ , and the oxygen-vacancy concentration is kept fixed for a particular stoichiometry with atomic precision, the use of  $\Delta\delta$  for chemical expansion coefficient is not very useful. Therefore, we have used the chemical expansion ( $\varepsilon_c$ ) variation with respect to the ionic radius ( $\Delta r$ ) of the substituted ion. Thus, Equation 9 is modified as

$$\alpha_c = \frac{\varepsilon_c}{\Delta r} \quad (10)$$

where  $\Delta r$  is change in the ionic radius of the substituted ion with respect to  $U^{4+}$  ion. For example, comparing the ionic radii of  $Ce^{4+}$  (0.97 Å) and  $U^{4+}$  (1.00 Å), the value of  $\Delta r = -0.03$  Å. Again Equation 8 can be compared with the coefficient of linear thermal expansion as

$$\frac{(a - a_0)}{a_0} = \alpha_T \Delta T$$

$$\frac{(a - a_0)}{a_0} = \alpha_C \Delta r \quad (11)$$

where  $\alpha_T$  is coefficient of linear thermal expansion,  $\Delta T$  is the change in temperature and  $\alpha_C$  is chemical expansion coefficient. Since, all the simulations are performed with single crystalline urania system, the variation in change in length is equivalent to measuring the change in lattice parameter

$$\frac{(a - a_0)}{a_0} = \frac{(L - L_0)}{L_0} \quad (12)$$

where  $L$  is the length of the supercell measured with substituted ions, and  $L_0$  is the length of the supercell for perfect  $UO_2$ . In addition to the above analysis, the  $\varepsilon_c$  values can be used to get an indication of the equivalent change in temperature ( $\Delta T_{eq}$ ) necessary to achieve the same amount of lattice parameter variation in pure  $UO_2$ . This is calculated by considering the  $\varepsilon_c$  values and the coefficient of thermal expansion reported for bulk  $UO_2$   $11.8 \times 10^{-6} K^{-1}$  15 from experiment, and using

$$\varepsilon_C = \alpha_{T, bulkUO_2} \Delta T_{eq} \quad (13)$$

### 3.3 $Ce^{4+}$ Substitution in $UO_2$

Before discussing the results on the effect of Lanthanide and Actinide substitution in  $UO_2$ , we have analyzed the atomistic model for  $Ce^{4+}$  substitution since experimental characterization of lattice parameter is available for  $U_{1-x}Ce_xO_2$  system Article11. Thus we used Pot1, Pot2 and Pot4 potentials to evaluate the change in lattice parameter for  $U_{1-x}Ce_xO_2$  system, where  $x < 0.3$ . It is important to note that Pot1, Pot2 and Pot4 are the only potentials which describe the  $Ce^{4+}$  ion interaction in  $UO_2$ .

Figure 2 illustrates the comparison of the relative change in lattice parameter with fraction of Ce. The relative change in lattice parameter is calculated with respect to the bulk  $UO_2$  lattice parameter predicted at  $x = 0$ . Following the results presented in Table 3, the lattice parameters predicted for pure  $UO_2$  are 5.4615 Å, 5.4681 Å, and 5.4749 Å for Pot1, Pot2, and Pot3 respectively. Comparing these lattice parameters, Pot2 quantitatively compares well with experiment (5.4698 Å Article11), while Pot1 underestimates and Pot4 overestimates the bulk  $UO_2$  lattice parameter. Therefore, a relative change in lattice parameter is more meaningful for comparison with experimental values of  $Ce^{4+}$  substitution.

Figure 2 clearly shows that all the potentials predicted the variation in lattice parameter of  $U_{1-x}Ce_xO_2$  system similar to experiment. Pot1 shows a larger deviation at larger concentration of  $Ce^{4+}$  in the urania matrix. Using the atomistic models we have successfully calculated the variation in structural property of a  $Ce^{4+}$  ion substituted urania system. Overall, the results show that substitution of a smaller ionic radius cation ( $Ce^{4+} = 0.97 \text{ \AA}$  compared to  $U^{4+} = 1.00 \text{ \AA}$ ) reduces the overall lattice parameter of the system.

These lattice variations predicted for the  $U_{1-x}Ce_xO_2$  system can be used to estimate the chemical expansion, expansion coefficient, change in lattice parameter and equivalent temperatures. Table 4 lists the comparison of chemical expansion and chemical expansion coefficients for  $U_{1-x}Ce_xO_2$  system. The predicted  $\epsilon_c$  and  $\alpha_c$  values with all the three empirical potentials are comparable to the experimental values for  $U_{1-x}Ce_xO_2$  system with  $x < 0.30$ . The results show that the lattice contraction observed for  $U_{0.72}Ce_{0.28}O_2$  system, is equivalent to reducing the temperature by  $\sim 273 \pm 31 \text{ K}$  for bulk  $UO_2$ . Similar analysis on  $Th^{4+}$  ions are recently published by Behera *et al.* 1.

### 3.4 Substitution of Other 4+ ions

Now we have considered the substitution of other 4+ Lanthanides and Actinides in urania ( $U_{1-x}A_xO_2$ ). The composition considered for substitution was 20% or  $U_{1-x}A_xO_2$ , where  $x=0.2$  and  $A = Am, Pu, Ce, Np,$  and  $Th$ . Figure 3 illustrates the variation in lattice parameter with ionic radii of the substituted A ions in the  $UO_2$  matrix. As ionic radius of the substituted ion increases, the lattice parameter increases. In Figure 3, we present the data with respect to the ionic radius of  $U^{4+}$ . Thus, the substitution of a lower ionic radius ion relative to  $U^{4+}$  ion decreases the overall lattice parameter, while a relatively larger ionic radius ion increases the average lattice parameter. This is in line with the discussion in Section 2, and the overall variation in lattice parameter is assigned to the elastic effect for 4+ ion substitution.

### 3.5 Substitution of 3+ ions

For a fixed charge model, such as the one considered for this study, the substitution of 3+ ions in the  $UO_2$  system requires the generation of oxygen vacancies in order to achieve a charge neutral system. Due to the change in charge of the substituted ion and the ionic radius, both elastic and electrostatic effects are present in  $U_{1-2x}A_{2x}O_{2-x}$  system. Here "A" may be the Lanthanides and Actinides substituted in the  $UO_2$  matrix or may be  $U^{3+}$ , which has a significantly higher radius than  $U^{4+}$ . First the effect of  $U^{3+}$  ion substitution is discussed followed by the effect of other 3+ Lanthanides and Actinides.

**$U^{3+}$  ion substitution:** The overall effect of  $U^{3+}$  ion substitution on the lattice parameter is illustrated in Figure 4. This figure plots the variation of lattice parameter with substitution of  $U^{3+}$  in  $U_{1-2x}A_{2x}O_{2-x}$  giving, in this special case,  $UO_{2-x}$ . The maximum value of substitution characterized is  $x = 0.1$ , which corresponds to replacement of

20% of the original  $\text{UO}_2$  matrix by  $\text{U}^{3+}$  and vacancies. The predicted variation of lattice parameter for  $\text{UO}_{2-x}$  system shows an overall increase in the lattice parameter with increase in  $x$ . This increase can be explained due to the larger ionic radii of the  $\text{U}^{3+}$  ion, and the reduced electrostatic attraction.

Figure 5 shows the variation in elastic constants due to the change in lattice parameter and the  $\text{U}^{3+}$  substitution. Due to the increase in the lattice parameter, it is expected that the  $\text{UO}_{2-x}$  will be mechanically softer than  $\text{UO}_2$ , which is evident from the moduli predictions for the  $\text{UO}_{2-x}$  system. The bulk modulus varies by  $\sim 29\%$ , and the Young's modulus decrease by  $\sim 43\%$  for  $\text{UO}_{1.90}$  (or 20%  $\text{U}^{3+}$  substitution).

Lanthanide 3+ and Actinide 3+ ion substitution: Here the elastic and electrostatic effect of 3+ Lanthanide and Actinide substitution is studied for  $\text{U}_{0.80}\text{A}_{0.20}\text{O}_{1.90}$ , which corresponds to  $x = 0.1$  and allows for direct comparison with the 4+ ion substitution corresponding to  $\text{U}_{0.80}\text{A}_{0.20}\text{O}_{2.00}$ . Figure 6 illustrates the change in lattice parameter with ionic radii of the substituted ions for  $\text{U}_{0.80}\text{A}_{0.20}\text{O}_{1.90}$ . The results show that lattice parameter increases with the increase in ionic radius of the substituted 3+ ion. The change in lattice parameter in Figure 6 can be directly compared with Figure 3 for 4+ ion substitution. The rate of increase in the lattice parameter for 3+ ions is relatively less than the 4+ ions. However, In Figure 6,  $\text{Nd}^{3+}$ ,  $\text{Pu}^{3+}$ ,  $\text{Ce}^{3+}$  and  $\text{U}^{3+}$  ions do not follow the lattice parameter variation trend. These ions show a larger change in ionic radius ( $> 10\%$ ) compared to the host  $\text{U}^{4+}$  ( $\text{U}^{4+} = 1.00 \text{ \AA}$ ,  $\text{Nd}^{3+} = 1.109 \text{ \AA}$ ,  $\text{Pu}^{3+} = 1.14 \text{ \AA}$ ,  $\text{Ce}^{3+} = 1.143 \text{ \AA}$ , and  $\text{U}^{3+} = 1.165 \text{ \AA}$ ). These larger ions lead to a greater strain in the lattice, which causes the observed deviation in the overall lattice parameter. Figure 7 shows the variation in bulk modulus as a function of ionic radii. The bulk moduli values show  $\sim 13\text{-}16\%$  reduction in the bulk modulus values, thereby reducing the mechanical properties. Shear and Young's moduli values show similar reduction of  $17\text{-}23\%$  and  $19\text{-}24\%$  respectively.

## 2. Discussions and Conclusions

The effect of 4+ and 3+ ion substitutions are combined to analyze the overall effect on lattice parameter of the urania matrix. This is achieved by plotting the 20% cation substitution in the urania matrix for both 4+ and 3+ ions. In effect this combines the results shown in Figures 3 and 6. The resultant Figure 8 illustrates that most of the Lanthanide and Actinide 4+ ions (except  $\text{Th}^{4+}$ ) decreases the overall lattice parameter, which is guided by the smaller size of the substituted 4+ ions compared to  $\text{U}^{4+}$ . However, all the 3+ ions increase the lattice parameter of the urania matrix.

Using Equation 8, the average chemical expansion is estimated for all the Lanthanides and Actinides considered in this study. Figure 9(a) plots the change in chemical expansion with the ionic radii of the substituted ions. Both 3+ and 4+ ions are considered, and show a linear trend with chemical expansion increasing with increase in ionic radius. Even though the slopes are similar, 4+ and 3+ ions do not follow the same line (between  $\text{Th}^{4+} = 1.05 \text{ \AA}$ , and  $\text{Gd}^{3+} = 1.053 \text{ \AA}$ ). This deviation can be

attributed to the additional electrostatic effect and oxygen vacancies associated with the 3+ ions substitution.

The chemical expansion coefficient is estimated by Equation 10 and is presented in Figure 9(b) as a function of ionic radius. This plot shows that most of the 4+ ions have a larger chemical expansion coefficient than the 3+ ions. The chemical expansions observed for 20% substitution have been used to estimate the equivalent temperatures in pure  $\text{UO}_2$  (Figure 10). For example, considering the effect of Am substitution, the observed chemical expansion is equivalent to decreasing the temperature by  $\sim 290$  K for  $\text{Am}^{4+}$ , and increasing the temperature by  $\sim 520$  K for  $\text{Am}^{3+}$  in pure  $\text{UO}_2$ . The deviation between 4+ and 3+ ions are observed between  $\text{Th}^{4+}$  ( $\Delta r = +0.050$  Å) and  $\text{Gd}^{3+}$  ( $\Delta r = +0.053$  Å). The equivalent temperatures are estimated to be  $+391$  K and  $+221$  K for  $\text{Th}^{4+}$  and  $\text{Gd}^{3+}$  respectively. We also estimated the effect of concentration on the equivalent temperatures. Figure 11 illustrates the variation in equivalent temperatures for three different concentrations ( $x = 0.03, 0.10, \text{ and } 0.20$ ). The absolute magnitudes of the equivalent temperatures increase with an increase in the concentration of the substituted ions.

Figure 12 shows the effect of substitution on bulk modulus. Most of the 4+ ions increase the bulk modulus of the urania matrix, which can be explained by the decrease in lattice parameter for 4+ ion substitution. Similarly most of the 3+ ions decrease the bulk modulus. For example, if we consider 20% substitution of americium in  $\text{UO}_2$  matrix,  $\text{Am}^{4+}$  increases the bulk modulus by  $<1\%$ , while  $\text{Am}^{3+}$  reduces the bulk modulus by  $\sim 16\%$ .

Thus, this paper shows how atomic level simulations can investigate the effect of structural and elastic property variation with substitution in  $\text{UO}_2$ . The incorporation of Lanthanides and Actinides in the urania matrix affects various thermo-physical properties such as elastic properties, thermal conductivity, ionic diffusion, phase stability. This paper has investigated the Lanthanide and Actinide substitution in  $\text{UO}_2$  matrix. We defined chemical expansion and the chemical expansion coefficient that relates the change in lattice parameter with ionic substitution. We then used this parameter to estimate the effect of 3+ and 4+ Lanthanide and Actinide substitution in the  $\text{UO}_2$  matrix. The results show that the structural and elastic properties are dependent on the elastic and electrostatic effects. Elastic effects are prominent for 4+ ion substitution, while both elastic and electrostatic effects are important for 3+ ion substitution. Further it is seen that all the ions with smaller ionic radii than the  $\text{U}^{4+}$  ions reduce the lattice parameter, while ions with larger ionic radii than the  $\text{U}^{4+}$  ions increase the lattice parameter. The chemical expansions due to substitution are used to estimate the equivalent temperature required to obtain similar lattice variation in pure  $\text{UO}_2$ . This study provides atomic level understanding of the effect of substitution on elastic properties of the urania fuel and is useful for understanding the effect of fission products on  $\text{UO}_2$  properties, on the properties of mixed oxide fuels, and minor actinide based fuels used for reprocessing.

## References

- 1 R. K. Behera, and C. S. Deo. 2011. Effect of  $Ce^{4+}$  and  $Th^{4+}$  Ion Substitution in Uranium Dioxide. Materials Research Society, Boston, MA.
- Article2 J. von Pezold, A. Dick, M. Friak, and J. Neugebauer. 2010. Generation and performance of special quasirandom structures for studying the elastic properties of random alloys: Application to Al-Ti. *Physical Review B* 81 (9)
- 3 H. X. Xu, R. K. Behera, Y. L. Wang, F. Ebrahimi, S. B. Sinnott, E. D. Wachsman, and S. R. Phillpot. 2010. A critical assessment of interatomic potentials for ceria with application to its elastic properties. *Solid State Ionics* 181 (11-12):551-556.
- Article4 T. Uchida, T. Arima, K. Idemitsu, and Y. Inagaki. 2009. Thermal conductivities of americium dioxide and sesquioxide by molecular dynamics simulations. *Computational Materials Science* 45 (2):229-234.
- 5 K. Govers, S. Lemehov, M. Hou, and M. Verwerft. 2008. Comparison of interatomic potentials for UO<sub>2</sub> Part II: Molecular dynamics simulations. *Journal of Nuclear Materials* 376 (1):66-77.
- 6 K. Govers, S. Lemehov, M. Hou, and M. Verwerft. 2007. Comparison of interatomic potentials for UO<sub>2</sub>. Part I: Static calculations. *Journal of Nuclear Materials* 366 (1-2):161-177.
- 7 M. Osaka, J. Adachi, K. Kurosaki, M. Uno, and S. Yamanaka. 2007. Molecular dynamics study on defect structure of gadolinia-doped thoria. *Journal of Nuclear Science and Technology* 44 (12):1543-1549.
- 8 A. R. Cleave. 2006. Atomic scale simulations for waste form applications, Department of Materials, Imperial College, London.
- Article9 S. McIntosh, J. F. Vente, W. G. Haije, D. H. A. Blank, and H. J. M. Bouwmeester. 2006. Oxygen stoichiometry and chemical expansion of Ba<sub>0.5</sub>Sr<sub>0.5</sub>Co<sub>0.8</sub>Fe<sub>0.2</sub>O<sub>3-δ</sub> measured by in situ neutron diffraction. *Chemistry of Materials* 18 (8):2187-2193.
- 10 T. Arima, S. Yamasaki, Y. Inagaki, and K. Idemitsu. 2005. Evaluation of thermal properties of UO<sub>2</sub> and PuO<sub>2</sub> by equilibrium molecular dynamics simulations from 300 to 2000 K. *Journal of Alloys and Compounds* 400 (1-2):43-50.
- Article11 D. J. Kim, Y. W. Lee, and Y. S. Kim. 2005. The thermal conductivity and lattice parameter measurements in a low Ce content (U<sub>1-y</sub>Ce<sub>y</sub>)O<sub>2</sub> mixed oxide. *Journal of Nuclear Materials* 342 (1-3):192-196.
- 12 D. J. Green. 2004. *An Introduction to the Mechanical Properties of Ceramics*: Cambridge University Press.
- 13 J. D. Gale, and A. L. Rohlf. 2003. The general utility lattice program (GULP). *Molecular Simulation* 29:291-341.
- 14 M. Nadeem, M. J. Akhtar, R. Shaheen, M. N. Haque, and A. Y. Khan. 2001. Interatomic potentials for some binary oxides. *Journal of Materials Science and Technology* 17 (6):638-642.
- 15 J. K. Fink. 2000. Thermophysical properties of uranium dioxide. *Journal of Nuclear Materials* 279 (1):1-18.
- 16 J. D. Gale. 1997. GULP: A computer program for the symmetry-adapted simulation of solids. *Journal of the Chemical Society, Faraday Transactions* 93 (4):629-637.
- 17 R. W. Grimes, and G. Busker. 1996. Predicting the behaviour of fission products in the uranium-oxygen system. *Nuclear Energy-Journal of the British Nuclear Energy Society* 35 (6):403-410.

- 18 R. W. Grimes, and C. R. A. Catlow. 1991. THE STABILITY OF FISSION-PRODUCTS IN URANIUM-DIOXIDE. *Philosophical Transactions of the Royal Society a-Mathematical Physical and Engineering Sciences* 335 (1639):609-634.
- 19 R. Berman, T. S. Tully, J. Belle, and I. Goldberg. 1971. ASSESSMENT OF THERMAL CONDUCTIVITY OF HIGH-DENSITY THORIA-URANIA COMPOSITIONS (LWBR DEVELOPMENT PROGRAM). *Transactions of the American Nuclear Society* 14 (1):147-&.
- 20 R. D. Shannon, and C. T. Prewitt. 1969. Effective ionic radii in oxides and fluorides. *Acta Crystallographica Section B-Structural Crystallography and Crystal Chemistry B* 25:925-946.
- 21 B. G. Dick, and A. W. Overhauser. 1958. Theory of the dielectric constants of alkali halide crystals. *Physical Review* 112 (1):90-103.
- 22 R. A. Buckingham. 1938. The classical equation of state of gaseous helium, neon and argon. *Proceedings of the Royal Society of London Series A* 168 (A933):264-283.
- 23 P. M. Morse. 1929. Diatomic molecules according to the wave mechanics. II. Vibrational levels. *Physical Review* 34 (1):57-64.

**TABLES**Table 1. List of atomic interactions available for Actinides and Lanthanides produced during UO<sub>2</sub> fuel cycle with specific charge

	<b>Grimes01</b>	<b>Grimes02</b>	<b>Grimes03</b>	<b>Nadeem</b>	<b>Osaka</b>	<b>Uchida</b>
<b>Referred as</b>	<b>Pot1<sup>18</sup></b>	<b>Pot2<sup>17</sup></b>	<b>Pot3<sup>8</sup></b>	<b>Pot4<sup>14</sup></b>	<b>Pot5<sup>7</sup></b>	<b>Pot6<sup>Article4;10</sup></b>
<b>Actinides</b>						
Th				4+	4+	4+
U	4+	4+	4+ 3+	4+	4+	4+
Np					4+	
Pu		4+	4+ 3+		4+	
Am					4+	4+ 3+
Cm						
<b>Lanthanides</b>						
Ce	4+	4+ 3+		4+		
Nd			3+			
Pm						
Sm		3+	3+			
Eu			3+			
Gd		3+	3+		3+	

Table 2a. Interatomic potential parameters for core-shell models (Pot2, Pot3, and Pot4) used to simulate various Lanthanides and Actinides substitution in urania. All the potentials listed here are formal charge models.

Species	Buckingham parameters			Core-shell parameters			Ref.
	A [eV]	$\rho$ [Å]	C [eV·Å <sup>6</sup> ]	$q_{\text{core}}$ [e]	$q_{\text{shell}}$ [e]	$k_2$ [eV·Å <sup>-2</sup> ]	
Pot1 18							
O <sup>2-</sup> – O <sup>2-</sup>	108.00	0.3800	56.06	2.40	-4.40	296.80	
U <sup>4+</sup> – O <sup>2-</sup>	2494.20	0.34123	40.16	-2.54	6.54	98.24	
U <sup>4+</sup> – U <sup>4+</sup>	18600.00	0.27468	32.64				
Ce <sup>4+</sup> – O <sup>2-</sup>	1984.20	0.34940	26.44	11.30	-7.30	1957.00	
Ce <sup>4+</sup> – U <sup>4+</sup>	101860.00	0.24076	23.87				
Pot2 17							
O <sup>2-</sup> – O <sup>2-</sup>	9547.96	0.2192	32.0	0.04	-2.04	6.30	
U <sup>4+</sup> – O <sup>2-</sup>	1761.775	0.35642	0.0	4.10	-0.10	160.00	
Pu <sup>4+</sup> – O <sup>2-</sup>	1682.08	0.3542	0.0	4.00			
Ce <sup>4+</sup> – O <sup>2-</sup>	1809.68	0.3547	20.40	4.20	-0.20	177.84	
Ce <sup>3+</sup> – O <sup>2-</sup>	2010.18	0.3449	23.11	3.00			
Sm <sup>3+</sup> – O <sup>2-</sup>	1944.44	0.3414	21.49	3.00			
Gd <sup>3+</sup> – O <sup>2-</sup>	1885.75	0.3399	20.34	3.00			
Pot3 8							
O <sup>2-</sup> – O <sup>2-</sup>	9547.96	0.2192	32.0	0.04	-2.04	32.00	
U <sup>4+</sup> – O <sup>2-</sup>	1761.775	0.356421	0.0	4.00			
Pu <sup>4+</sup> – O <sup>2-</sup>	1762.84	0.35420	11.48	4.00			
U <sup>3+</sup> – O <sup>2-</sup>	1165.65	0.376582	0.0	3.00			
Pu <sup>3+</sup> – O <sup>2-</sup>	1150.745	0.37430	12.10	3.00			
Nd <sup>3+</sup> – O <sup>2-</sup>	1995.20	0.34300	22.59	3.00			
Sm <sup>3+</sup> – O <sup>2-</sup>	1944.44	0.34140	21.49	3.00			
Eu <sup>3+</sup> – O <sup>2-</sup>	1925.71	0.34030	20.59	3.00			
Gd <sup>3+</sup> – O <sup>2-</sup>	1885.75	0.3399	20.34	3.00			
Pot4 14							
O <sup>2-</sup> – O <sup>2-</sup>	25.41	0.6937	32.32	0.513	-2.513	20.53	
U <sup>4+</sup> – O <sup>2-</sup>	9296.65	0.2796	90.00	5.00	-1.00	134.00	
Th <sup>4+</sup> – O <sup>2-</sup>	8638.50	0.2856	70.00	4.64	-0.64	110.00	
Ce <sup>4+</sup> – O <sup>2-</sup>	7549.87	0.2831	70.00	2.75	1.25	222.00	

Table 2b. Interatomic potential parameters for rigid ion models (Pot5 and Pot6) used to simulate various Lanthanides and Actinides substitution in urania. All the potentials listed here are partial charge models.

Species	Buckingham parameters			Morse parameters			Ref.
	A [eV]	$\rho$ [Å]	C [eV·Å <sup>6</sup> ]	D [eV]	$\beta_{ij}$ [1/Å]	$r^*_{ij}$ [Å]	
<b>Pot5 7</b>							
O <sup>1.2-</sup> – O <sup>1.2-</sup>	2346.1488	0.32	4.14616				
U <sup>2.4+</sup> – U <sup>2.4+</sup>	442.2081	0.32	0.0				
U <sup>2.4+</sup> – O <sup>1.2-</sup>	1018.5705	0.32	0.0	0.78101	1.25	2.369	
Th <sup>2.4+</sup> – Th <sup>2.4+</sup>	17.0261	0.82	0.0				
Th <sup>2.4+</sup> – O <sup>1.2-</sup>	61.4295	0.57	0.0	1.21500	1.90	2.360	
Np <sup>2.4+</sup> – Np <sup>2.4+</sup>	20027.9343	0.16	0.0				
Np <sup>2.4+</sup> – O <sup>1.2-</sup>	4530.9265	0.24	0.0	0.45559	3.27	2.339	
Pu <sup>2.4+</sup> – Pu <sup>2.4+</sup>	32610.2942	0.16	0.0				
Pu <sup>2.4+</sup> – O <sup>1.2-</sup>	5330.4009	0.24	0.0	0.56406	1.56	2.339	
Am <sup>2.4+</sup> – Am <sup>2.4+</sup>	3568.4382	0.16	0.0				
Am <sup>2.4+</sup> – O <sup>1.2-</sup>	2549.5744	0.24	0.0	0.37315	3.98	2.339	
Gd <sup>1.8+</sup> – Gd <sup>1.8+</sup>	139021.40	0.16	0.0				
Gd <sup>1.8+</sup> – O <sup>1.2-</sup>	8643.0870	0.24	0.0	1.27132	0.80	2.353	
<b>Pot6 Article4;10</b>							
O <sup>1.35-</sup> – O <sup>1.35-</sup>	919.17	0.332	17.36				
U <sup>2.7+</sup> – U <sup>2.7+</sup>	2.48 x 10 <sup>+13</sup>	0.072	0.0				
U <sup>2.7+</sup> – O <sup>1.35-</sup>	55918.39	0.202	0.0				
Th <sup>2.7+</sup> – O <sup>1.35-</sup>	31321.23	0.220	0.0				
Am <sup>2.7+</sup> – Am <sup>2.7+</sup>	2.73 x 10 <sup>+12</sup>	0.075	0.0				
Am <sup>2.7+</sup> – O <sup>1.35-</sup>	42635.38877	0.203	0.0				
Am <sup>2.025+</sup> – Am <sup>2.025+</sup>	5.69 x 10 <sup>+15</sup>	0.060	0.0				
Am <sup>2.025+</sup> – O <sup>1.35-</sup>	68417.58793	0.196	0.0				

Note that due to the partial charge definitions for Pot5 all the +4 charges are defined as an effective charge of +2.4 e and the +3 charges are assigned +1.8 e; while for Pot6 the corresponding charges are +2.7 e and +2.025 e respectively.

**Table 3.** Comparison of bulk properties of UO<sub>2</sub> calculated from different interatomic potentials with experiment.

	<b>Experiment</b>	<b>Pot1</b>	<b>Pot2</b>	<b>Pot3</b>	<b>Pot4</b>	<b>Pot5</b>	<b>Pot6</b>
Lattice parameter [Å]	5.4698	5.4615	5.4681	5.4682	5.4749	5.4654	5.4449
Lattice Energy (eV/ThO <sub>2</sub> )	-106.700	-105.6762	-104.502	-104.501	-107.479	-45.589	-51.005
C <sub>11</sub> [GPa]	389	524	532	532	626	419	434
C <sub>12</sub> [GPa]	119	147	122	122	187	59	120
C <sub>44</sub> [GPa]	60	89	121	122	144	55	109
Poisson's ration		0.219	0.187	0.187	0.230	0.124	0.217
Compressibility [10 <sup>-3</sup> /GPa]		3.66	3.86	3.86	3.00	5.58	4.45
Static Dielec. Const.	24.0	13.1	18.1	7.8	19.1	3.8	3.2
High. Freq. Di Const.	5.3	5.3	5.7	2.0	4.9		
Phonons at $\Gamma$ (293 K)							
T. mode (cm <sup>-1</sup> )	280.0	344.0	178.9	294.9	238.4	295.0	379.5
L. mode (cm <sup>-1</sup> )	450.0	533.3	282.2	444.6	427.6	577.2	570.7
Anisotropy factor (Z)	0.44	0.47	0.59	0.59	0.66	0.30	0.69
B <sub>single_crystal</sub> [GPa]	204	273	259	259	333	179	225
G <sub>single_crystal</sub> [GPa]		113	150	150	171	90	126
Y <sub>single_crystal</sub> [100] [GPa]	385	459	486	486	540	405	382
Y <sub>single_crystal</sub> [111] [GPa]*	170	218	287	289	354	123	265
B <sub>polycrystal</sub> [GPa]	204	273	259	259	333	179	225
G <sub>polycrystal</sub> [GPa]	77-90	113-129	145-155	145-155	167-174	76-105	124-128
Y <sub>polycrystal</sub> [100] [GPa]	205-235	298-334	366-387	367-387	429-445	199-263	314-323

\* Young's modulus along [111] direction is calculated using Z values. Berman and Belle reported the value of Z = 0.47 for UO<sub>2</sub>.

Table 4. Chemical expansion coefficients calculated for Ce<sup>4+</sup> ion substitution in U<sub>1-x</sub>Ce<sub>x</sub>O<sub>2</sub> system using Pot1, Pot2 and Pot4 potentials compared to experiment Article11. The symbols:  $x$  is the concentration of substituted ion,  $a_0$  is the lattice parameter of UO<sub>2</sub> perfect lattice,  $a$  is the lattice parameter measured at a particular concentration,  $\Delta a$  is change in the lattice parameter,  $\varepsilon_c$  is change chemical expansion,  $\Delta r$  is change in the ionic radius,  $\alpha_c$  is the chemical expansion coefficient, and  $\Delta T_{eq}$  is the equivalent temperature.

	$x$	$a_0$ (Å)	$a$ (Å)	$\Delta a$ (Å)	$\varepsilon_c$	$\Delta r$ (Å)	$\alpha_c$ (Å <sup>-1</sup> )	$\Delta T_{eq}$ (K)*
Experiment	0	5.4698						
	0.0763		5.4653	-0.0045	-0.0008	-0.03	0.027	-70
	0.1484		5.4607	-0.0091	-0.0017	-0.03	0.055	-141
	0.2168		5.4577	-0.0121	-0.0022	-0.03	0.074	-187
	0.2817		5.4530	-0.0168	-0.0031	-0.03	0.102	-260
Pot1	0	5.4615						
	0.06		5.4577	-0.0039	-0.0007	-0.03	0.024	-60
	0.15		5.4510	-0.0105	-0.0019	-0.03	0.064	-163
	0.21		5.4470	-0.0145	-0.0027	-0.03	0.089	-226
	0.28		5.4418	-0.0197	-0.0036	-0.03	0.120	-306
Pot2	0	5.4681						
	0.06		5.4650	-0.0031	-0.0006	-0.03	0.019	-49
	0.15		5.4596	-0.0085	-0.0016	-0.03	0.052	-132
	0.21		5.4565	-0.0117	-0.0021	-0.03	0.071	-181
	0.28		5.4524	-0.0157	-0.0029	-0.03	0.096	-244
Pot4	0	5.4749						
	0.06		5.4714	-0.0035	-0.0006	-0.03	0.021	-54
	0.15		5.4655	-0.0094	-0.0017	-0.03	0.057	-146
	0.21		5.4620	-0.0129	-0.0024	-0.03	0.079	-200
	0.28		5.4575	-0.0174	-0.0032	-0.03	0.106	-270

\*The value of  $\Delta T_{eq}$  is calculated based on experimental thermal expansion coefficient of UO<sub>2</sub> ( $\alpha_T = 11.8 \times 10^{-6} \text{ K}^{-1}$ ) [FINK 2000 JNM]

Table 5. Chemical expansion coefficients calculated for +4 ion substitution in  $U_{0.80}A_{0.20}O_2$  system ( $x = 0.20$ ) using empirical potentials (for the meaning of the symbols please refer Table 4).

Potential	$a_0$ (Å)	A ion	$\Delta r$ (Å)	$a$ (Å)	$\epsilon_C$	$\alpha_C$ (Å <sup>-1</sup> )	$\Delta T_{eq}$ (K)*
Pot1	5.4681	Ce <sup>4+</sup>	-0.03	5.4476	-0.0026	0.085	-217
Pot2	5.4681	Pu <sup>4+</sup>	-0.04	5.4502	-0.0033	0.082	-279
		Ce <sup>4+</sup>	-0.03	5.4569	-0.0021	0.068	-174
Pot3	5.4682	Pu <sup>4+</sup>	-0.04	5.4541	-0.0026	0.064	-218
Pot4	5.4749	Ce <sup>4+</sup>	-0.03	5.4625	-0.0023	0.076	-192
		Th <sup>4+</sup>	+0.05	5.4984	+0.0043	0.086	+364
Pot5	5.4654	Am <sup>4+</sup>	-0.05	5.4479	-0.0032	0.064	-271
		Pu <sup>4+</sup>	-0.04	5.4505	-0.0027	0.068	-231
		Np <sup>4+</sup>	-0.02	5.4620	-0.0006	0.031	-53
		Th <sup>4+</sup>	+0.05	5.4877	+0.0041	0.082	+345
Pot6	5.4449	Am <sup>4+</sup>	-0.05	5.4252	-0.0036	0.073	-307
		Th <sup>4+</sup>	+0.05	5.4747	+0.0055	0.109	+463

\*The value of  $\Delta T_{eq}$  is calculated based on experimental thermal expansion coefficient of  $UO_2$  ( $\alpha_T = 11.8 \times 10^{-6} K^{-1}$ ) [FINK 2000 JNM]

Table 6. Chemical expansion coefficients calculated for +3 ion substitution in  $U_{0.80}A_{0.20}O_{1.90}$  system ( $x = 0.20$ ) using empirical potentials (for the meaning of the symbols please refer Table 4).

Potential	$a_0$ (Å)	A ion	$\Delta r$ (Å)	$a$ (Å)	$\epsilon_C$	$\alpha_C$ (Å <sup>-1</sup> )	$\Delta T_{eq}$ (K)*
Pot2	5.4681	Gd <sup>3+</sup>	0.053	5.4784	+0.0019	0.036	+159
		Sm <sup>3+</sup>	0.079	5.4894	+0.0039	0.049	+330
		Ce <sup>3+</sup>	0.143	5.5073	+0.0072	0.050	+607
Pot3	5.4682	Gd <sup>3+</sup>	0.053	5.4824	+0.0026	0.049	+221
		Eu <sup>3+</sup>	0.066	5.4872	+0.0035	0.053	+295
		Sm <sup>3+</sup>	0.079	5.4932	+0.0046	0.058	+389
		Nd <sup>3+</sup>	0.109	5.5007	+0.0060	0.055	+504
		Pu <sup>3+</sup>	0.140	5.6599	+0.0351	0.250	+2971
		U <sup>3+</sup>	0.165	5.6771	+0.0382	0.232	+3238
<b>Pot5</b>	<b>5.4654</b>	<b>Gd<sup>3+</sup></b>	<b>0.053</b>				
Pot6	5.4449	Am <sup>3+</sup>	0.090	5.4785	+0.0062	0.068	+522

\*The value of  $\Delta T_{eq}$  is calculated based on experimental thermal expansion coefficient of  $UO_2$  ( $\alpha_T = 11.8 \times 10^{-6} K^{-1}$ ) [FINK 2000 JNM]

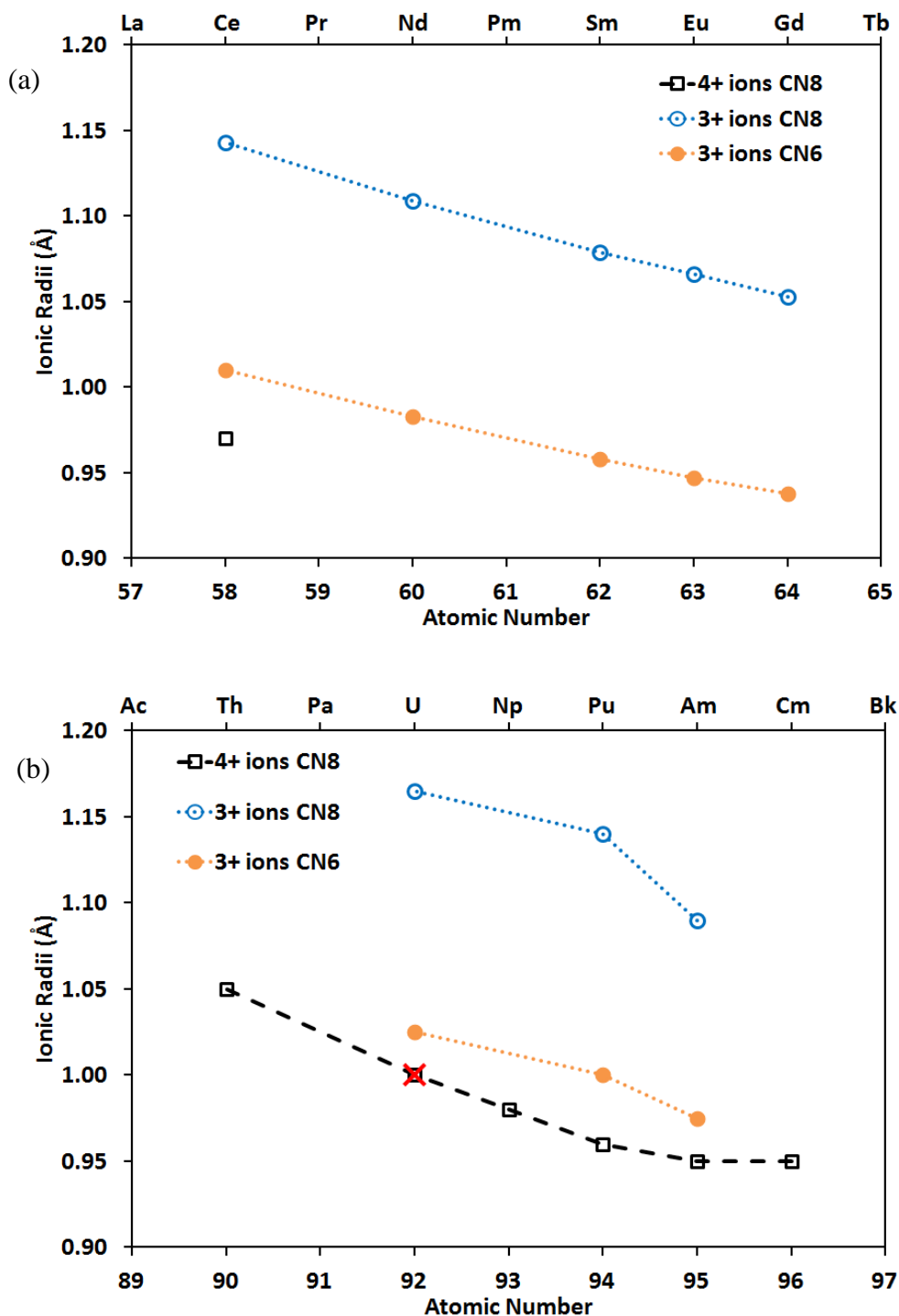
**Figures**

Figure 1: Shannon ionic radii of 4+ ions with 8 coordination number and 3+ ions with 8 and 6 coordination numbers for (a) Lanthanides, and (b) Actinides. The data with the red cross in (b) represents the ionic radius of  $U^{4+}$  ion (1.0 nm).

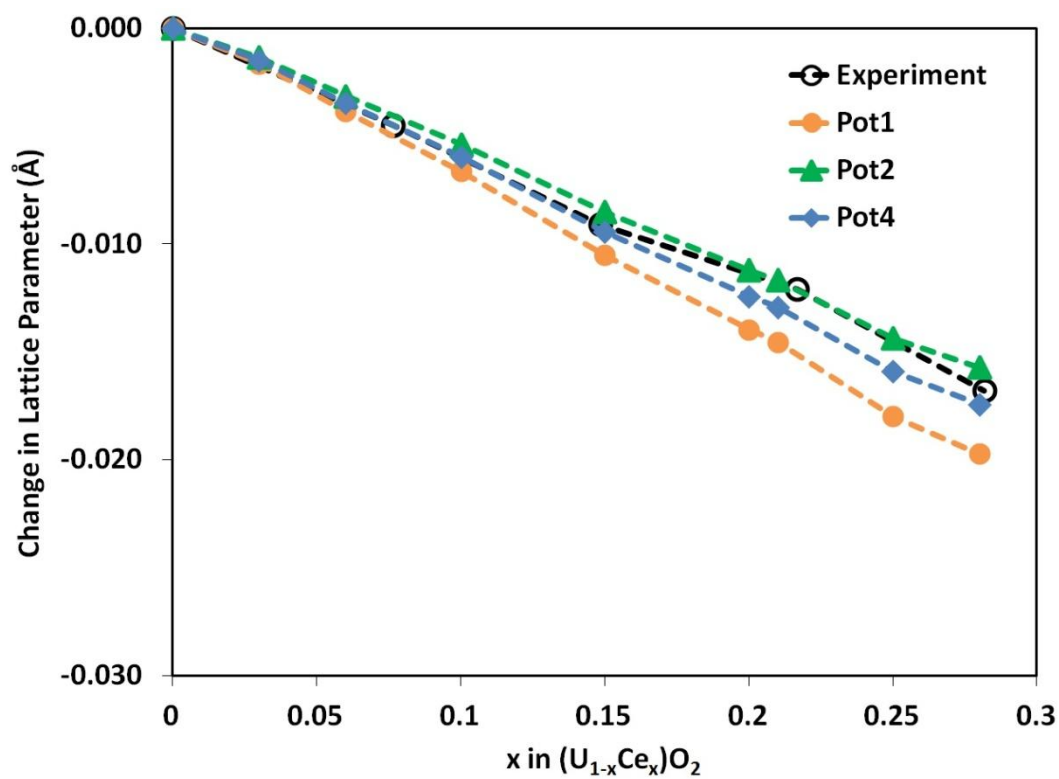


Figure 2 : Relative variation of lattice parameter due to 4+ ion substitution in  $U_{1-x}Ce_xO_2$  system with respect to the bulk  $UO_2$  lattice parameter.

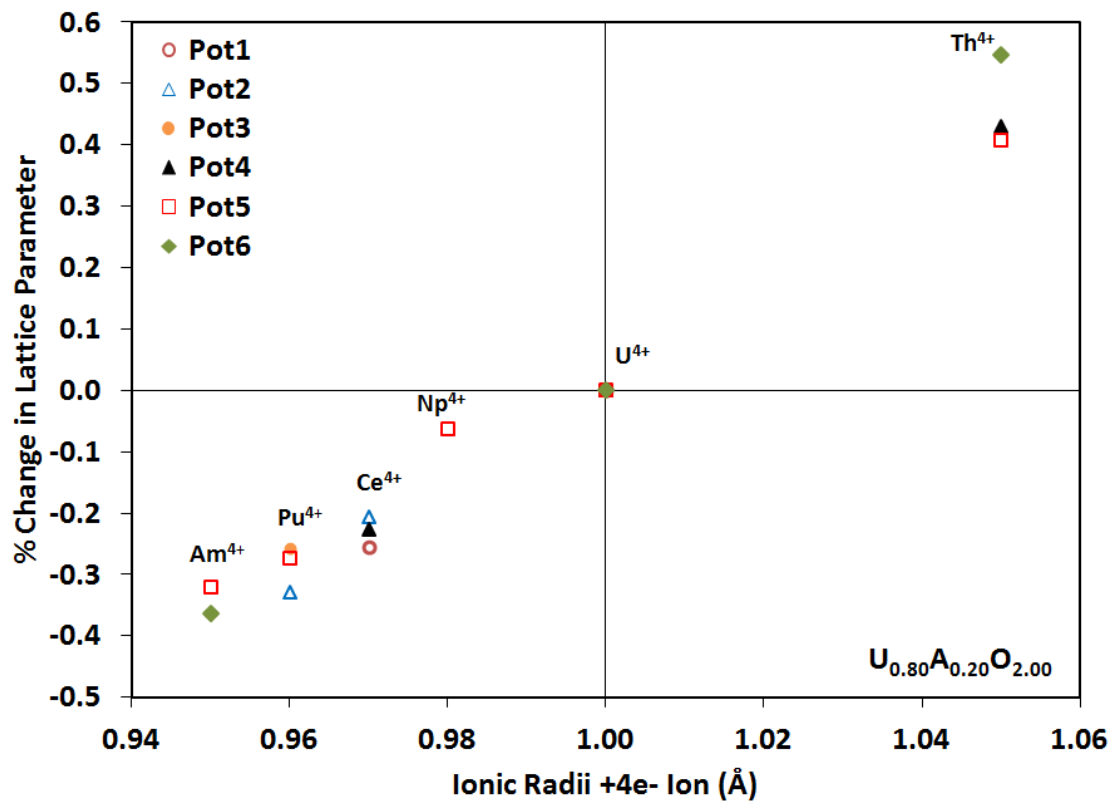


Figure 3: Variation of lattice parameter due to 4+ ion substitution in  $U_{1-x}A_xO_2$  system, where  $x = 0.20$ .

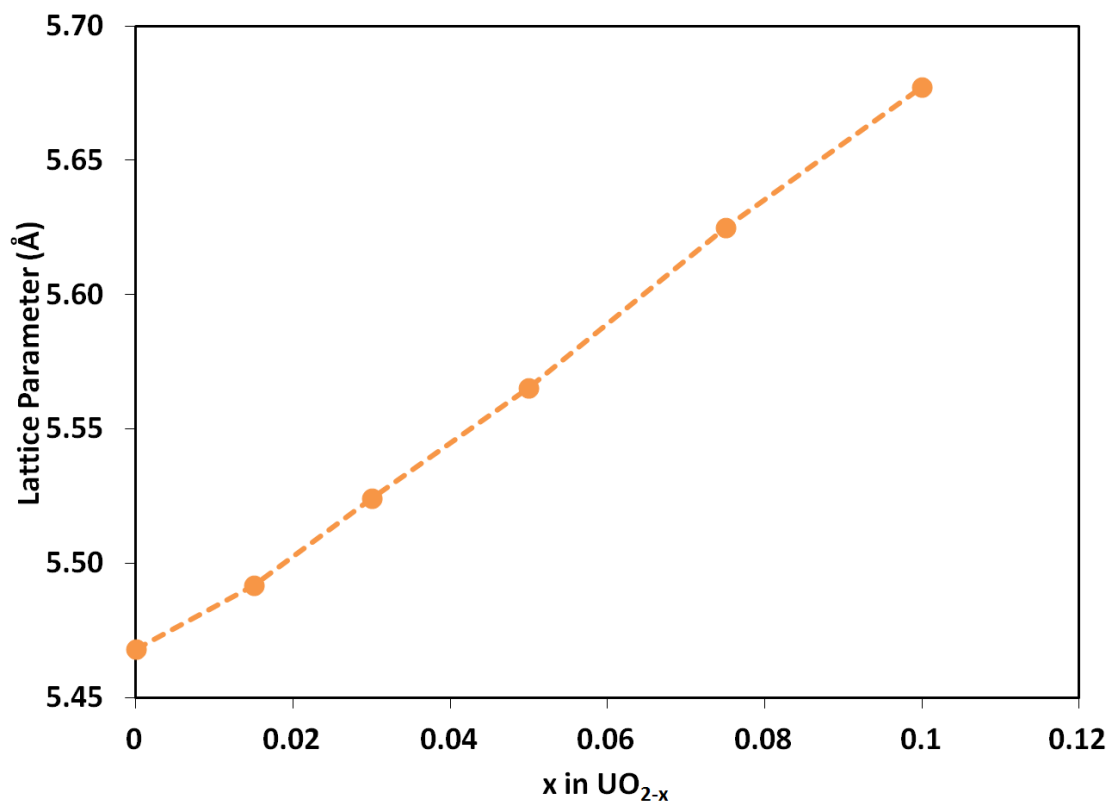


Figure 4: Variation of lattice parameter due to  $\text{U}^{3+}$  ion substitution in  $\text{UO}_{2-x}$  system using Pot3. Pot3 is the only potential which can describe  $\text{U}^{3+}$  ion substitution.

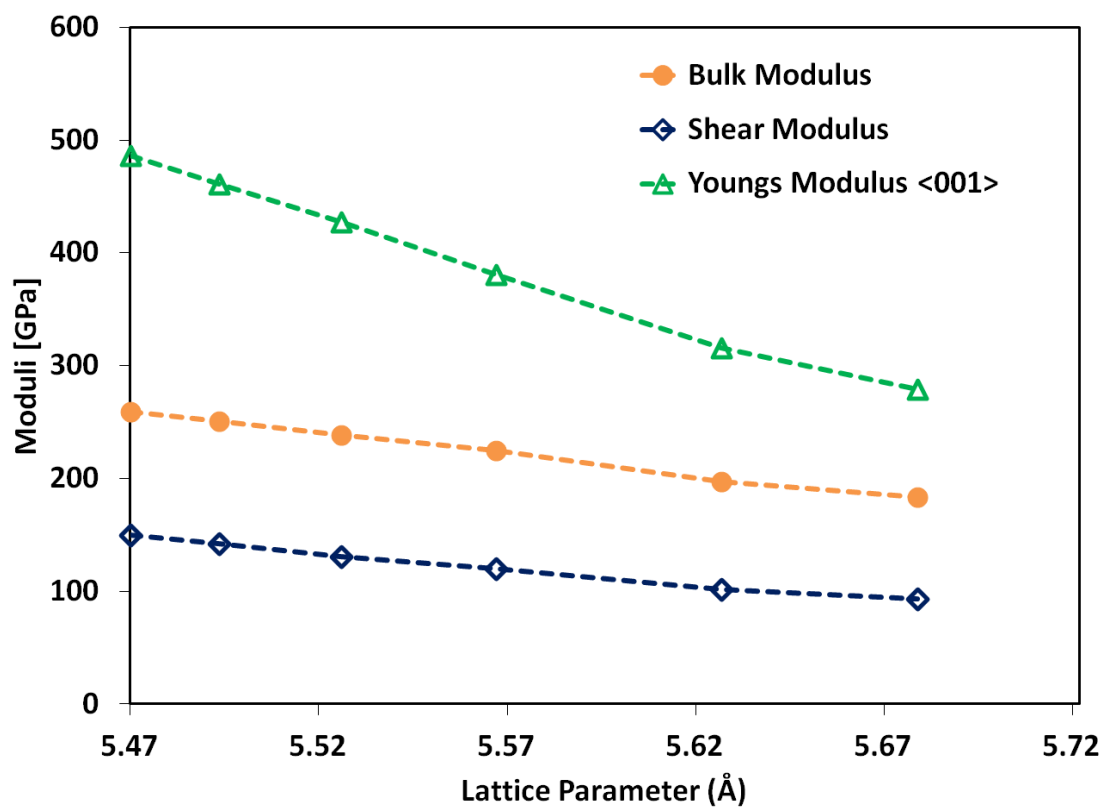


Figure 5: Variation of bulk, shear, and Young's modulus in  $\text{UO}_{2-x}$  system using Pot3.

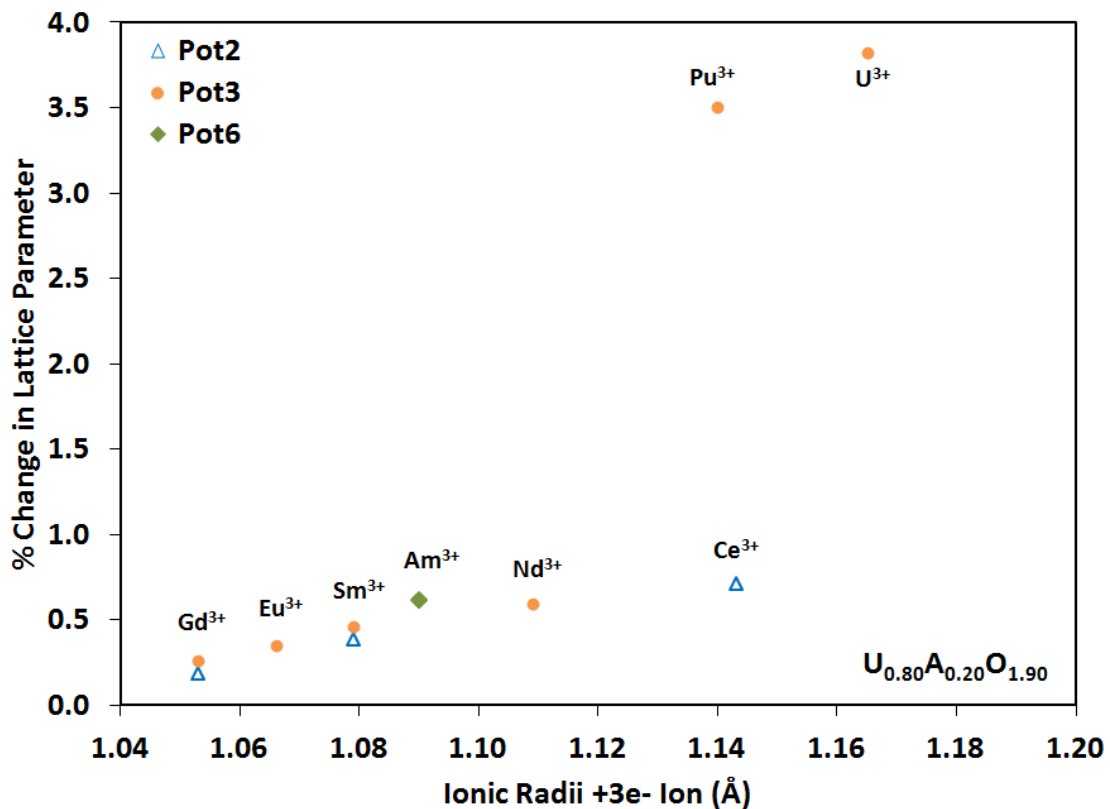


Figure 6: Variation of lattice parameter due to 3+ ion substitution in  $U_{1-2x}A_{2x}O_{2-x}$  system, where  $2x = 0.20$ .

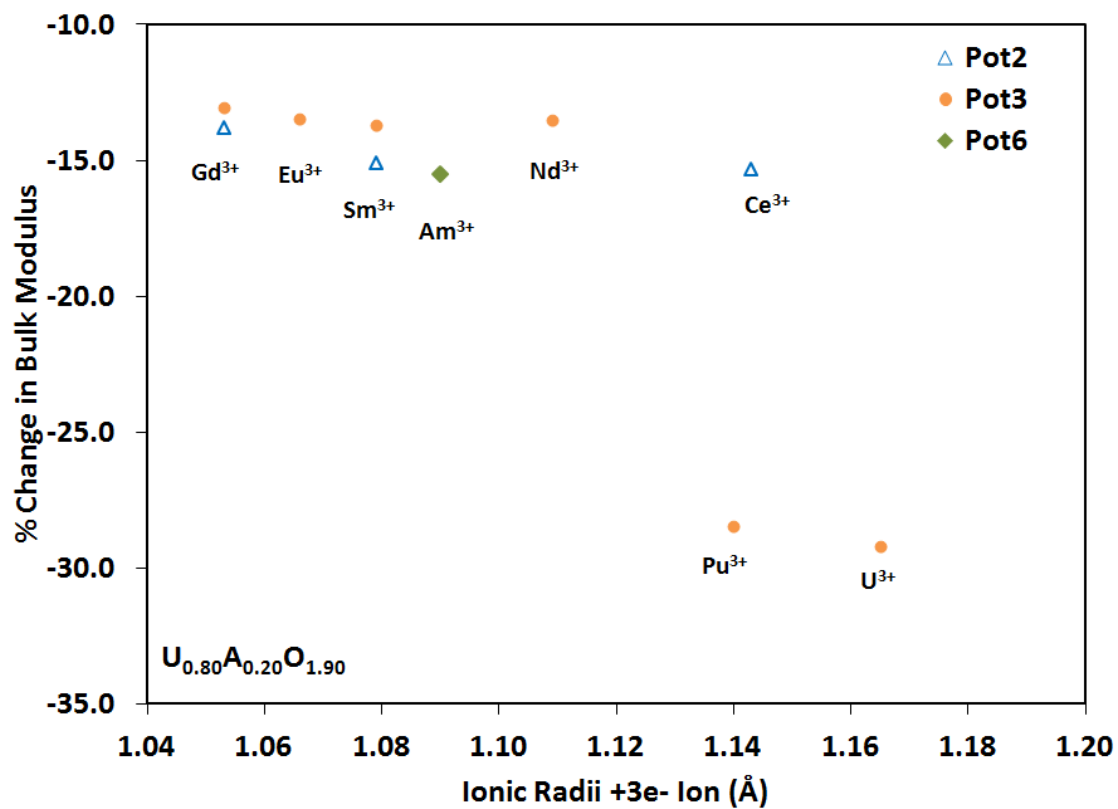


Figure 7: Variation of bulk modulus due to 3+ ion substitution in  $U_{1-2x}A_{2x}O_{2-x}$  system, where  $2x = 0.20$ .

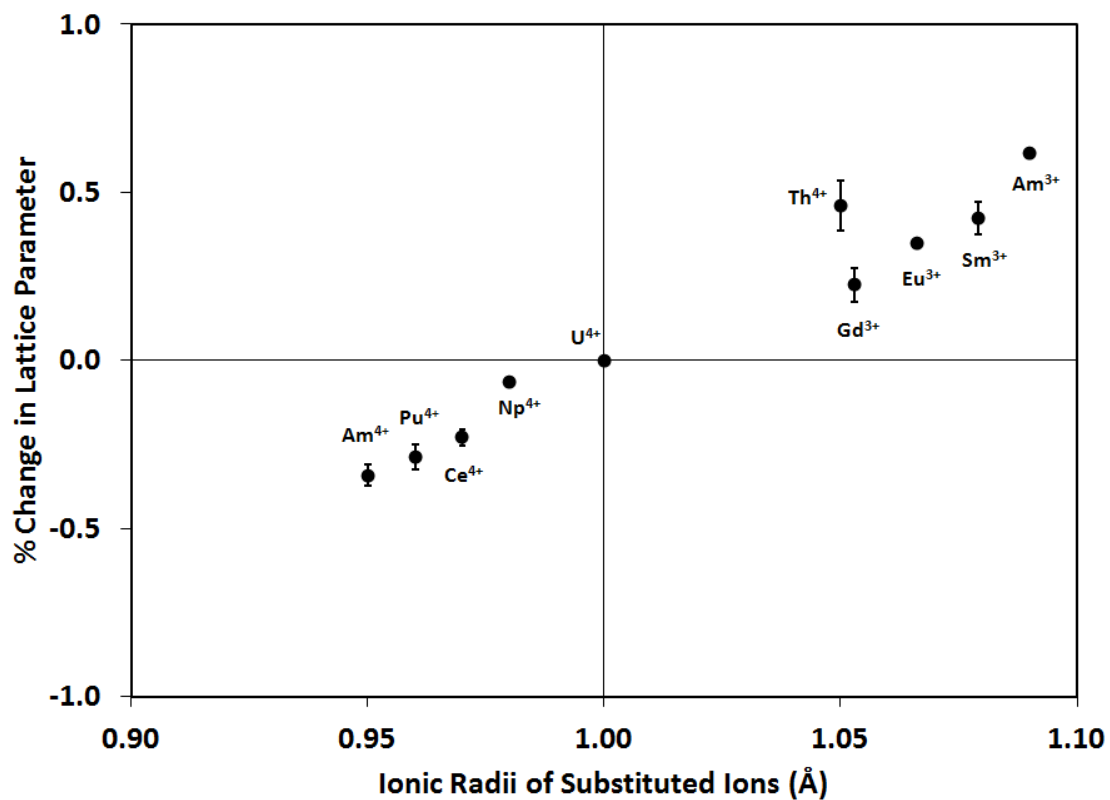


Figure 8: Effect of 4+ and 3+ ion substitutions in uranium dioxide, where the stoichiometric fraction of A is 0.20.

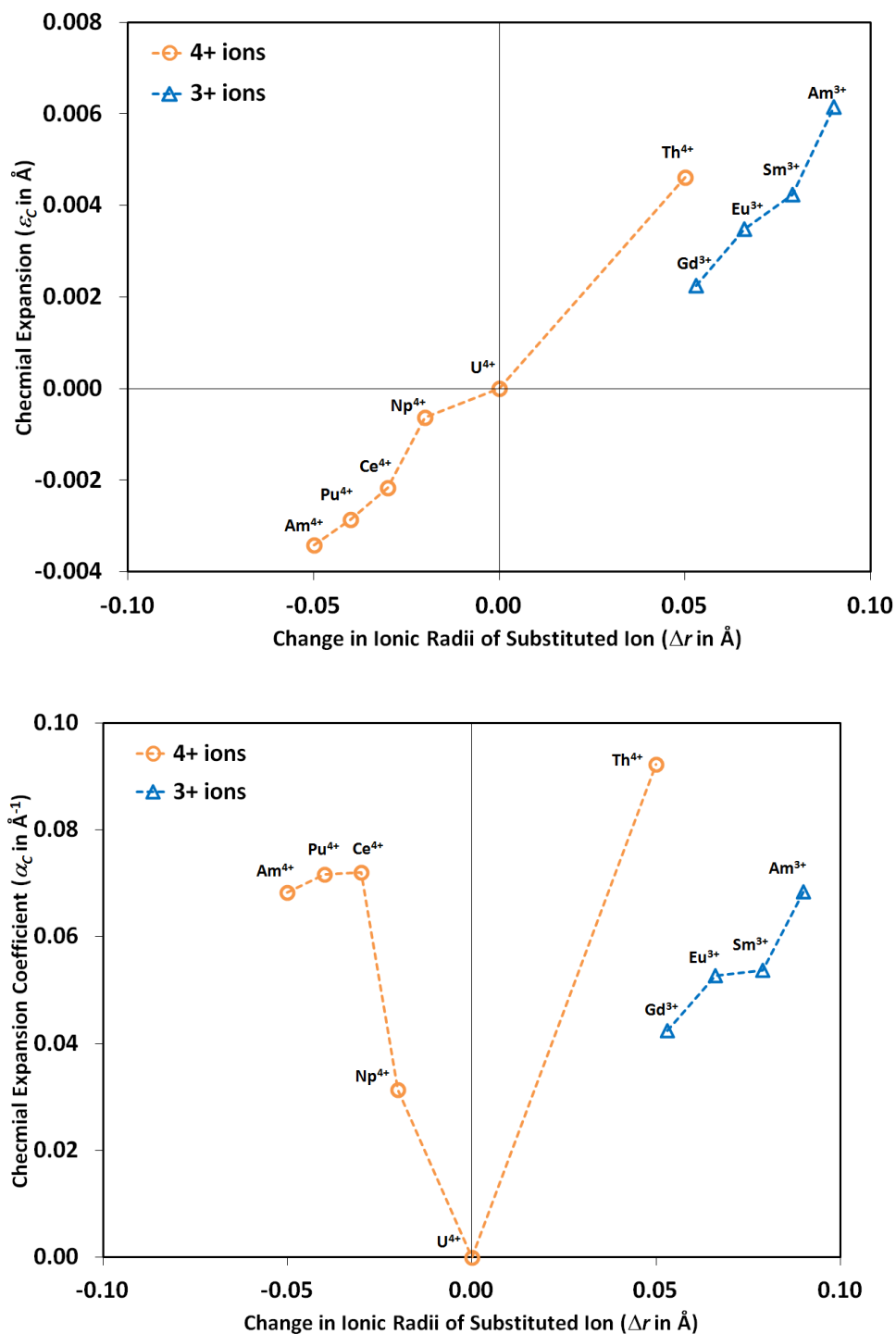


Figure 9: Comparison of (a) chemical expansion ( $\epsilon_C$ ) and (b) chemical expansion coefficient ( $\alpha_C$ ) of 4+ and 3+ ion substitution in  $U_{0.80}A_{0.20}$  system. The ( $\epsilon_C$ ) increases with an increase in the substituted ionic radii with respect to  $U^{4+}$  ionic radius, and vice versa. The ( $\alpha_C$ ) is always positive and increases with the increase in the magnitude of the change in ionic radii.

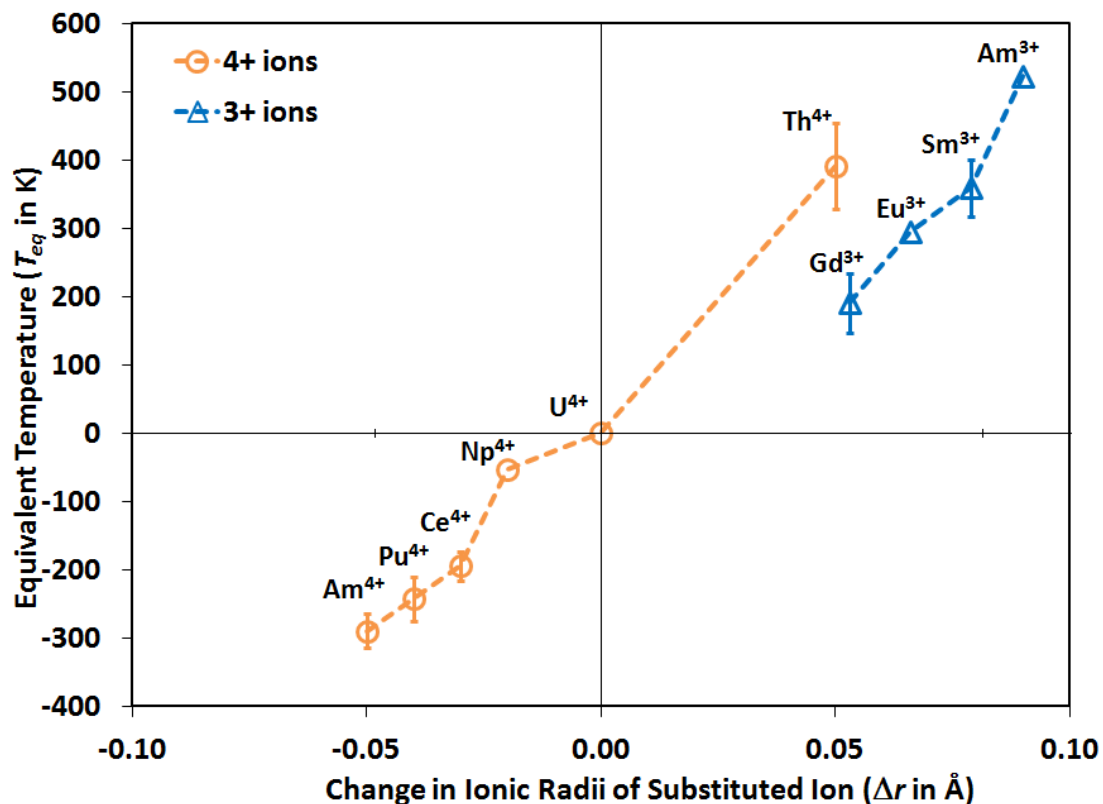


Figure 10: The calculated equivalent temperature ( $T_{eq}$ ) for each type of substituted specie in  $UO_2$  to achieve an equal amount of lattice expansion or contraction in a perfect  $UO_2$  lattice. The experimental linear thermal expansion coefficient was used to derive these temperatures.

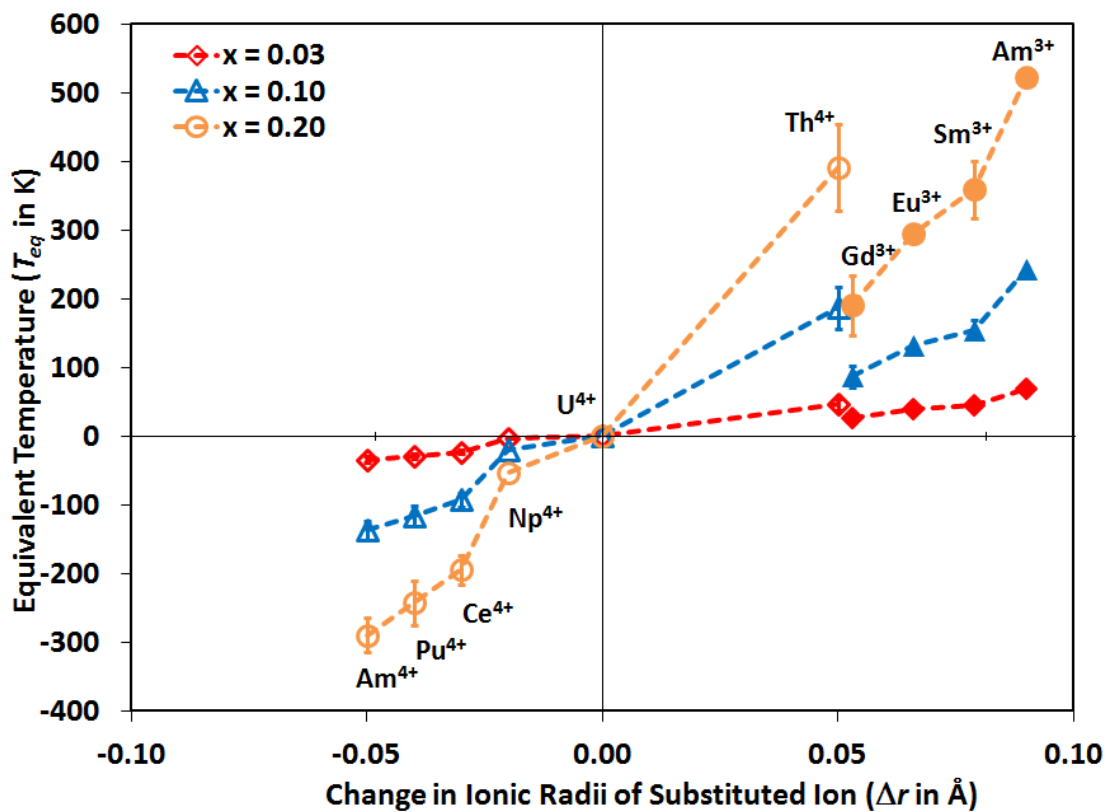


Figure 11: The effect of concentration on the equivalent temperature ( $T_{eq}$ ) for each type of substituted specie in  $UO_2$ . The open symbols are for 4+ ions and solid symbols are for 3+ ions. The magnitude of  $T_{eq}$  increases with an increase in concentration.

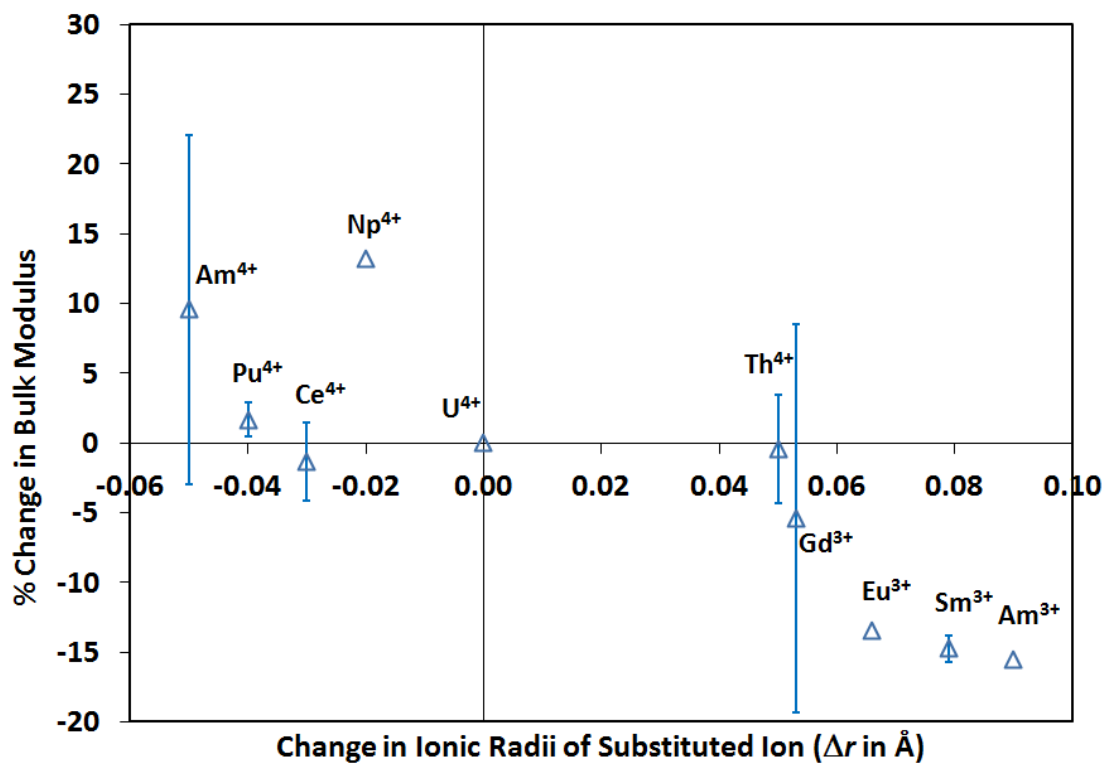


Figure 12: The % change in bulk modulus calculated for each type of substituted specie in UO<sub>2</sub>. Most of the 4+ ions increase the bulk modulus while most of the 3+ ions reduce the bulk modulus.

## Appendix 2:

### **Development of (U,Th)O<sub>2</sub> interatomic potentials**

Critical assessments of several available UO<sub>2</sub> empirical potentials are summarized by Govers *et al.* [2, 3]. In particular, they have characterized static properties [2] (elastic constants, bulk modulus, Young's modulus, dielectric constants, phonon frequencies and defect formation energies), and dynamics properties [3] (temperature evolution of different elastic properties) of UO<sub>2</sub> predicted by different interatomic potentials (nearly 20).

In comparison to UO<sub>2</sub>, there are only a few ThO<sub>2</sub> empirical potentials available in the literature. The first interatomic potential description of UO<sub>2</sub> and ThO<sub>2</sub> is reported by Benson *et al.* [4]. This is a rigid-ion model, which was used to calculate the cohesive energy, elastic properties and surface energies of ThO<sub>2</sub>. However, the complete potential parameters used to calculate the properties are not available in the article. Mackrodt *et al.* [5] and Colbourn *et al.* [6] are next to simulate ThO<sub>2</sub> using interatomic potentials. Colbourn *et al.* performed an extensive analysis of defect properties of ThO<sub>2</sub> using interatomic potential in 1983. However, both these articles did not provide the parameters used for interatomic potentials. Clausen *et al.* [7] developed a potential based on the phonon dispersion relationship of ThO<sub>2</sub>. Even though the potential parameters are available, the potential model by Clausen *et al.* is very difficult to investigate ThO<sub>2</sub> properties. To the best of our knowledge, Nadeem *et al.* [8] and Osaka *et al.* [9] are the only other literature providing empirical potential parameters to analyze the properties of ThO<sub>2</sub>. These two potentials are referred as NASHK and OAKUY [10] from hereinafter. A brief summary of all the articles characterizing properties of ThO<sub>2</sub> using interatomic interactions are listed in Table 1.

Our approach in this article is to develop several empirical potentials, which will be used to investigate the static and dynamic properties of ThO<sub>2</sub>. In particular, we selected the O-O interactions of the UO<sub>2</sub> rigid-ion models described by Tharmlingam [11], Walker *et al.* [12], Lewis *et al.* [13], Sindzingre *et al.* [14], Karakasidis *et al.* [15], Basak *et al.* [16], Morelon *et al.* [17], and Arima *et al.* [18] (the sequence follows the year the article was published). Th-Th interactions and Th-O interactions are developed and fit to lattice parameter, elastic constants and the static dielectric constants.

This paper is organized as follows: Section 2 provides the information on the potential description of ionic oxides for atomic level simulations. This section also discusses our approach towards developing different interatomic interactions. Section 3 deals with the results and discussion, where we have compared the predicted elastic properties, phase stability, defect and surface stabilities by each empirical potential with available experimental, first-principles and empirical models. A critical assessment of the potential models is discussed in Section 4, followed by a summary

presented in Section 5.

## 1. Methodology

Figure 1 illustrates the crystal structure of ThO<sub>2</sub>, where Th-ions occupy the face centered positions and O-ions occupy the tetrahedral sites. This ionic arrangement belongs to the Fluorite structure with  $Fm\bar{3}m$  symmetry (space group # 225). Since the bonding in ThO<sub>2</sub> is predominantly ionic, for atomic level simulations the long-range interactions are described by the Coulombic interaction, whereas the short-range interactions are described predominantly by strong repulsive interactions.

### 2.1 Short range interactions

One of the most common forms of short-range interaction used for ionic systems is the Buckingham potential [19, 20]:

$$V_{Buck}(r_{ij}) = A_{ij} \exp(-r_{ij}/\rho_{ij}) - C_{ij}/r_{ij}^6 - D_{ij}/r_{ij}^8 \quad (1)$$

where  $r_{ij}$  is the separation between two ions  $i$  and  $j$ ; and  $A$ ,  $\rho$ ,  $C$  and  $D$  are free parameters, which physically represent the pair-wise repulsion coefficient between the electron clouds; the ionic radii of the atoms; and the van der Waals attraction between the core and the electrons of the interacting atoms.

In addition to the Buckingham potential, there are a few other short-range potentials which can be used for ionic oxides. One such interaction is the Buckingham-4 potential, which attempts to avoid the unphysical attractive forces at very short distances. This is given as:

$$V_{Buck-4}(r_{ij}) = \begin{cases} A_{ij} \exp(-r_{ij}/\rho_{ij}) & \text{if } r_{ij} \leq r_1 \\ 5^{th} \text{ order polynomial} & \text{if } r_1 < r_{ij} \leq r_{min} \\ 3^{rd} \text{ order polynomial} & \text{if } r_{min} < r_{ij} \leq r_2 \\ -C_{ij}/r_{ij}^6 & \text{if } r_{ij} > r_2 \end{cases} \quad (2)$$

where  $r_{ij}$  is the separation between two ions  $i$  and  $j$ ; and  $A$ ,  $\rho$ ,  $C$ ,  $r_1$ ,  $r_{min}$ , and  $r_2$  are free parameters.

The other such short-range interaction is given by the Morse potential [21], which is used to describe the covalent bonding in the system. The Morse potential is given as:

$$V_{Morse}(r_{ij}) = D_{ij} \left\{ \left[ 1 - \exp(-\beta_{ij}(r_{ij} - r_{ij}^*)) \right]^2 - 1 \right\} \quad (3)$$

where  $r_{ij}$  is the separation between two ions  $i$  and  $j$ ; and  $D$ ,  $\beta$  and  $r_{ij}^*$  are free parameters.

### 2.2 Long Range Interactions

The other type of distinction in the model definition can be described by the charges on the ions. For ThO<sub>2</sub> a +4 charge on Th and -2 charge on oxygen is a formal charge model. Any other charge definition on Th and O ions are called a partial charge model. In order to include polarization of the ions, a shell model description

can be used to define the ions. In the shell model [22], each ion is described by a core and a shell, the sum of whose charges is the ionic charge. The core and shell on each ion is attached to each other via a spring (which can be harmonic or anharmonic). A shell model where the core and shell of an atom are coupled by a harmonic spring is given by:

$$V(\omega) = \frac{1}{2}k_2\omega^2 \quad (4)$$

where  $\omega$  is the core-shell displacement, and  $k_2$  is the harmonic spring constants.

The pair interactions necessary for simulating ThO<sub>2</sub> are Th-Th, Th-O, and O-O. . ThO<sub>2</sub> interatomic potential descriptions

The potentials are developed by fitting the experimental lattice parameter, elastic constants and static dielectric constant. A least square method is used to measure the best fit obtained with the specific weighting factors used for the experimental parameters. The developed potential parameters are tested to obtain positive phonon frequencies for the fluorite structure. The General Utility Lattice Program (GULP) [23, 24] was used to investigate the properties of the ThO<sub>2</sub> potentials.

This fitting procedure resulted in nine interatomic potential models to describe ThO<sub>2</sub> referred to hereafter as BD01, BD02, ..., BD09 [10]. Table 2 summarizes the list of developed potentials with brief information regarding the UO<sub>2</sub> models. The O-O interaction described by Sindzingre *et al.* [14], Karakasidis *et al.* [15] are the same for UO<sub>2</sub>. Therefore, the ThO<sub>2</sub> interaction developed for these two models are the same and referred as BD05 They will differ if used to described the ThO<sub>2</sub>-UO<sub>2</sub> mixed system.

Table 3 provides the potential parameters for all the ThO<sub>2</sub> models used to characterize ThO<sub>2</sub> in this article. Most of the potentials are formal charge models ( $q_{\text{Th}} = +4.0e^-$ , and  $q_{\text{O}} = -2.0e^-$ ), except OAKUY, BD06, BD07 and BD09, which are partial charge models. The literature potential NASHK is the only shell model potential used in this article. Thus a total of eleven interatomic potentials are used to characterize various static properties of ThO<sub>2</sub>.

## 2. Results and Discussions

In this section we have calculated static properties of ThO<sub>2</sub> with all the pair potentials, and compared the properties with available experimental and first-principles results. The discussions are focused on the structural and elastic properties, phase stability, defect energetic and surface energies predicted by each potential.

### 3.1 Structure and Elastic Properties

In order to estimate lattice parameter, the ThO<sub>2</sub> Fluorite structure is geometrically optimized by each potential till all the atoms in the unit cell experience net zero force. Elastic properties are calculated by analyzing the energy-volume relationship with the applied strain in the system. Appropriate strains in the x, y and z directions are applied and the elastic constants obtained from the stress-strain relations. The bulk

modulus is calculated by analyzing the energy response of an equal strain applied along all the three directions of the optimized bulk system, while Young's modulus is calculated by applying strain along a particular direction. The results predicted from each potential are compared with the experimental values (Table 4).

First we will focus on the properties calculated by NASHK and OAKUY potentials. Both the potentials underestimate the lattice parameter ( $\sim 0.09\%$  for NASHK and  $\sim 0.36\%$  for OAKUY). The NASHK potential overestimates all the individual elastic constants by more than 50% compared to the experimental values, thereby overestimating the bulk modulus and shear modulus by  $> 50\%$ . The potential overestimates the Young's modulus by  $\sim 94\%$ . The NASHK potential does predict the static (within 0.25%) and high-frequency dielectric constants (underestimates by  $\sim 8\%$ ) quite accurately. As the only core shell model considered, it is the only one that can predict the high frequency dielectric constant. Similar analysis on the OAKUY potential shows a much improved bulk and shear modulus (within 15%) prediction. The Young's modulus was overestimated by  $\sim 60\%$ . This model underestimates the static-dielectric constant by  $\sim 85\%$ .

For all the potentials developed by us (BD 01-09 in Table 2), the lattice parameter is calculated within 0.01% error ( $-0.004\%$  for BD04, and BD06;  $0.002\%$  for BD08;  $0.003\%$  for BD01;  $0.004\%$  for BD02;  $0.005\%$  for BD03, and BD05;  $0.006\%$  for BD07; and  $\sim 0.008\%$  for BD09). The fitted elastic constants ( $C_{11}$ , and  $C_{12}$ ) are well within 0.3% range, while  $C_{44}$  is overestimated by all the potentials ( $\sim 4.4\%$  for BD06;  $\sim 13.2\%$  for BD02 and BD07; and  $> 20\%$  for rest of the potentials). This improved description of the elastic constants resulted in a better description of the moduli values. The bulk modulus is underestimated by  $\sim 3\%$ , while the shear modulus is overestimated by  $\sim 15\%$  (BD06 potential underestimates the shear modulus by  $\sim 1\%$ ). The Young's modulus is within 25% (which is typical of empirical potentials) for all the potentials.

Similar analysis on the Poisson's ratio shows an underestimation of  $\sim 20\%$  by all the potentials, except OAKUY ( $\sim 37\%$ ). The static dielectric constants are severely underestimated by all the rigid ion models. The shell-model description by NASHK is the only model which described the dielectric constants close to experiment. Overall, the lattice parameter and elastic properties predicted by the developed  $\text{ThO}_2$  potentials are observed to be better than the published NASHK and OAKUY potentials.

### 3.2 Phase Stability

Phase stability is critical, as nuclear fuel materials are subjected to high temperature and pressure during application. Thus, all the potentials are used to predict the ground state phase stability of  $\text{ThO}_2$  based on a variety of  $\text{AB}_2$  structures at zero temperature and pressure. We have computed 11 different phases, which follow the work on  $\text{TiO}_2$  by Swamy and Gale [25]. The different phases considered are Anatase (Tetragonal space group:  $I41/amd$ , #141), Baddeleyite (Monoclinic, space group:  $P21/c$ , #14), Brookite (Orthorhombic, space group:  $Pbca$ , #61), Columbite (Orthorhombic, space group:  $Pbcn$ , #60), Cotunnite (Orthorhombic, space group:

*Pnma*, #62), Fluorite (Cubic, space group: *Fm-3m*, #225), Hollandite (Tetragonal space group: *I4/m*, #87), Pyrite (Cubic, space group: *Fm-3m*, #205), Ramsdellite (Orthorhombic, space group: *Pnma*, #62), Rutile (Tetragonal space group: *P4/2mm*, #136), TiO<sub>2</sub>B (Monoclinic, space group: *C2/m*, #12). One unit cell of Rutile contains 2 ThO<sub>2</sub> units; one unit cell of Anatase, Baddeleyite, Columbite, Cotunnite, Fluorite, Pyrite and Ramsdellite contains 4 ThO<sub>2</sub> units; while one unit cell of Brookite, Hollandite and TiO<sub>2</sub>B structures contain 8 ThO<sub>2</sub> units.

Table 5 illustrates the predicted phase stability of ThO<sub>2</sub> with all the interatomic descriptions. The energy of each crystal structure is calculated relative to the fluorite structure (eV/ThO<sub>2</sub>). A positive value in the relative energy indicates the structures are less favorable and a negative value represents the structures to be more favorable than the Fluorite structure. For most of the potentials, the fluorite AO<sub>2</sub> structure is predicted to be the most stable structure (Fig. 2). However, the BD06 potential predicted Cotunnite (model - PbCl<sub>2</sub>) structure to be more favorable. The kinetic barrier (not calculated in this article) between different phases will be a key factor for any phase transformation observed in the presence of any external field (temperature, stress or electric field).

All the ThO<sub>2</sub> potentials developed in this study have the common O-O interactions with the respective UO<sub>2</sub> potentials from the literature. Thus, we evaluate the phase stabilities predicted for UO<sub>2</sub> using the original UO<sub>2</sub> interatomic potentials as defined in table 2 (Fig. 3). Table 6 summarizes the results obtained for the polymorphs of UO<sub>2</sub>. From the relative energy calculations only NASHK, Lewis (BD04 for ThO<sub>2</sub>), Morelon (BD07 for ThO<sub>2</sub>) and Arima2 (BD09 for ThO<sub>2</sub>) predicted the Fluorite phase to be the most favorable. The Cotunnite phase is predicted to be energetically favorable by Basak potential, which is the same for the BD06 potential for ThO<sub>2</sub>. The rest of the UO<sub>2</sub> potentials predicted multiple AO<sub>2</sub> polymorphs to be more stable than the Fluorite phase. Therefore, care must be taken while performing high-temperature and high-pressure calculations for UO<sub>2</sub> using these potentials. Thus, the developed ThO<sub>2</sub> potentials using the O-O interactions of the UO<sub>2</sub> descriptions substantially improved the predicted phase order.

In addition to the above discussion, the potential BD07 based on the Morelon [17] UO<sub>2</sub> O-O interaction was only suitable for calculating bulk properties. The potential description could not optimize the different AO<sub>2</sub> phases correctly. This characteristic of the BD07 potential can be attributed to the limited fitting parameters used in our approach. The original UO<sub>2</sub> potential was developed by fitting the lattice parameter and defect energies. In this work, we use minimal fitting parameters - lattice parameter, elastic constants and the static dielectric constant. Based on this approach, BD07 fails to calculate defect properties, i.e., its transferability is poor. More input fitting parameters are necessary to develop Th-O, and Th-Th interactions which will be suitable to investigate various properties of ThO<sub>2</sub>. The BD07 potential is not employed to calculate defect and surface properties of ThO<sub>2</sub>.

### 3.3 Defect Formation Energies

We have calculated the defect formation energies focusing on the point defects: Th-vacancy ( $V_{\text{Th}}$ ), Th-interstitial ( $\text{Th}_i$ ), O-vacancy ( $V_{\text{O}}$ ), and O-interstitial ( $\text{O}_i$ ); and defect complexes (Schottky, Cation Frenkel, Anion Frenkel, Divacancy and Tetravacancy). The generation of point defects in  $\text{ThO}_2$  creates a charged system, and defects can cause very long range structural perturbations. The Mott-Littleton approach is used to calculate the defect energies, where the crystal with defect is divided into three regions, Regions 1, 2a and 2b. Region 1 is the volume that contains the defects, while region 2b is the bulk region and Region 2a is the transition between Regions 1 and 2b. A complete local relaxation is performed for Region 1 and some atomic relaxation is allowed for Region 2a. Performing an energy convergence test, the size of Regions 1 and 2a are defined as 14 Å and 20 Å respectively in a 4 x 4 x 4 supercell for all the defect calculations.

Table 7 summarizes the predicted defect formation energies of point defects and complex defects considered in this study. In a unit cell of  $\text{ThO}_2$ , vacancies are generated by removing one atom of Th or O from the lattice site. The formation energies of interstitials are calculated by placing a Th or O atom in the body-centered site of the  $\text{ThO}_2$  unit cell. Comparing the formation energies of point defects, interstitials are relatively more favorable than vacancies. All the potentials predict the point defect stability to be  $\text{Th}_i < \text{O}_i < V_{\text{O}} < V_{\text{Th}}$ , similar to the point defect energies predicted by Catlow [26] for  $\text{UO}_2$ . The BD01 and BD02 potentials failed to optimize the structures with point defects. Therefore, these two potentials are not used to calculate the defect complexes. Based on the current analysis, BD01 and BD02 should not be used for investigating defects in  $\text{ThO}_2$ . The other potentials predict the defect properties within reasonable values of the experimental and previously published calculations.

Following the work by Govers *et al.* [2] the formation energies of the neutral defect complexes are calculated for different arrangements of the individual defects. Frenkel pairs are formed by the combination of a vacancy and interstitial of the same species. Thus, the energies for O-Frenkel and Th-Frenkel pairs are calculated for different arrangement of the vacancy and interstitial in the system. We consider three arrangements of the defect species for our study.

*IN the first case, we assume the Frenkel pairs to be at infinite distance ( $FP_{\infty}$ ):* These energies are estimated by using the individual point defect formation energies. For O-Frenkel at infinite distance ( $\text{OFP}_{\infty}$ ), the energy is estimated by adding the energies of O-Interstitial and O-vacancy predicted by each potential. Similar procedure is followed for Th-Frenkel ( $\text{ThFP}_{\infty}$ ) at infinite distance. *In the second arrangement, the O-Frenkel are very close to each other ( $\text{OFP}_1$  and  $\text{OFP}_2$ ):* For Frenkel pairs close to each other in the first nearest neighbor, the vacancies and interstitials recombine at the vacant lattice site. There are two different interstitial and vacancy arrangements considered for O-Frenkel pair. Considering the lattice Th atom (0, 0, 0) as the reference, the  $\text{O}_i$  occupied the  $(+\frac{1}{2}, +\frac{1}{2}, +\frac{1}{2})$  site. In order to avoid the recombination for  $\text{OFP}_1$  the  $V_{\text{O}}$  is at the  $(-\frac{1}{4}, -\frac{1}{4}, -\frac{1}{4})$  lattice site, and for  $\text{OFP}_2$  the  $V_{\text{O}}$  is at the  $(-\frac{1}{4}, -\frac{1}{4}, +\frac{1}{4})$  lattice site.

*For the third case of frenkel defect arrangements, the Th-Frenkel close to each other (ThFP<sub>1</sub>):* For Th-Frenkel, considering the lattice O atom (+1/4, +1/4, +1/4) as the reference, the Th<sub>i</sub> occupied the (+1/2, +1/2, +1/2) site and V<sub>Th</sub> is considered at the (-1/2, +1/2, 0) site. This Th-Frenkel is referred as ThFP<sub>1</sub> for discussion.

The formation energies of all the Frenkel pairs are listed in Table 7. Comparing the energies at infinite distance OFP<sub>∞</sub> are more stable than ThFP<sub>∞</sub>. The Frenkel pairs arranged close to each other are consistently more favorable than the pairs at infinite distance. OFP<sub>2</sub> is calculated to be the most favorable Frenkel pair in ThO<sub>2</sub>. This trend is same as the Frenkel pair energies predicted for UO<sub>2</sub> [2].

Schottky defects are formed when a stoichiometric unit of ThO<sub>2</sub> is missing in the lattice (one V<sub>Th</sub> and two V<sub>O</sub>). Two arrangements of Schottky defects are calculated for this study.

*The first arrangement has Schottky defect at infinite distance (Sch<sub>∞</sub>):* These energies are estimated by adding the individual point defect formation energies for V<sub>Th</sub> and V<sub>O</sub>.

- *In the second case, Schottky defects are close to each other (Sch<sub>1</sub>, Sch<sub>2</sub> and Sch<sub>3</sub>):* Three different vacancy arrangements are analyzed for Schottky defects close to each other. The V<sub>Th</sub> is considered at the (0, 0, 0) site and one of the V<sub>O</sub> is located at the (+1/4, +1/4, +1/4) site. The other V<sub>O</sub> position is varied for obtaining different vacancy arrangements. The V<sub>O</sub> site for Sch<sub>1</sub> is (-1/4, -1/4, -1/4), Sch<sub>2</sub> is (-1/4, +1/4, -1/4), and Sch<sub>3</sub> is (-1/4, +1/4, +1/4).

The formation energies of Schottky defects close to each other are relatively more favorable than Sch<sub>∞</sub>. Among the Schottky defects close to each other, the Sch<sub>1</sub> configuration is predicted to be energetically more favorable than Sch<sub>2</sub> and Sch<sub>3</sub> for most of the potentials (Table 7). The comparison of the formation energies of complex neutral defects at infinite distance resulted in anion Frenkel < Schottky < cation Frenkel, which is the same trend reported for UO<sub>2</sub> [2, 26].

While fixed charged empirical potentials provide critical qualitative information regarding defect stability, the absolute formation energies are generally predicted to be higher compared to experimental values or *ab initio* calculations. Crocombette [27] calculated the intrinsic point defect energies in ZrSiO<sub>4</sub> using both empirical and *ab initio* calculations. The study shows that empirical potentials overestimated the neutral defect complex energies by a factor of 1.5 – 1.9 compared to the *ab initio* calculations.

*Binding Energies:* In addition to the neutral defect complexes, we have also analyzed the binding energies of Diinterstitials, Divacancies, and Tetravacancy. These results will indicate the prediction of cluster formation with different potentials. There are three different diinterstitials considered Dii<sub>m</sub>, Dii<sub>O</sub>, and Dii<sub>Th</sub>. Dii<sub>m</sub> is the mixed Diintersitital (Th<sub>i</sub> + O<sub>i</sub>), Dii<sub>O</sub> is the oxygen Diinterstitial (O<sub>i</sub> + O<sub>i</sub>), Dii<sub>Th</sub> is the thorium Diinterstitial (Th<sub>i</sub> + Th<sub>i</sub>). All the interstitials are located at the body centered position of the Fluorite crystal structure.

a) Five different Divacancies are considered for discussion  $\text{Div}_m$ , 3 different  $\text{Div}_O$ , and  $\text{Div}_{Th}$ .  $\text{Div}_m$  is the mixed Divacancy ( $V_{Th} + V_O$ ), where the position of  $V_{Th}$  is at (0, 0, 0) and  $V_O$  is at (+1/4, +1/4, +1/4). For oxygen Divacancies one of the  $V_O$  is considered at (+1/4, +1/4, +1/4), and the other  $V_O$  is at (-1/4, -1/4, -1/4) for  $\text{Div}_{O1}$ , (-1/4, +1/4, -1/4) for  $\text{Div}_{O2}$ , and (-1/4, +1/4, +1/4) for  $\text{Div}_{O3}$ . Similarly  $\text{Div}_{Th}$  indicates the thorium Divacancy, where  $V_{Th}$  are located at (0, 0, 0) and (+1/2, +1/2, 0).

b) Also, a mixed tetravacancy ( $\text{Tetrav}_m$ )  $2V_{Th} + 2V_O$  is considered, where  $V_{Th}$  are located at (0, 0, 0) and (+1/2, +1/2, 0), and the  $V_O$  are at (+1/4, +1/4, +1/4) and (+1/4, +1/4, -1/4).

The binding energies of all the charged defect clusters are listed in Table 8. A positive binding energy indicates the cluster is more likely to form, while a negative binding energy indicates the cluster is unstable. Since, our model does not allow charges to change on the ions, all the similar ionic species clusters are energetically unstable ( $\text{Dii}_O$ ,  $\text{Dii}_{Th}$ ,  $\text{Div}_O$ ,  $\text{Div}_{Th}$ ). This characteristic can be attributed to the electrostatic repulsion between similar charged species. However, all the mixed clusters are energetically stable ( $\text{Dii}_m$ ,  $\text{Div}_m$ , and  $\text{Tetrav}_m$ ) with positive binding energies. Similar to  $\text{UO}_2$  [2, 28], Di-interstitials and Di-vacancies are the minimum defect clusters expected to form in  $\text{ThO}_2$ . Further investigation is necessary to characterize the defect clusters in  $\text{ThO}_2$  for the possibility of Willis clusters [29], or Di-interstitial clusters [28] as predicted for  $\text{UO}_2$ .

### 3.4 Surface Stability

In addition to the above properties, surface stability of  $\text{ThO}_2$  are investigated. Skomurski *et al.* [30] used a quantum-mechanical approach to investigate the stability of low-index  $\text{ThO}_2$  surfaces. In this study calculate the energies of (1 0 0), (1 1 0) and (1 1 1) surfaces with all the empirical potentials.

In order to simulate surfaces, we use a 3-D periodic unit cell containing an isolated, free-standing thin film (slab) with a vacuum region of  $\sim 30 \text{ \AA}$  (Fig. 4). The vacuum region prevents any artificial interactions of one surface with the other through the periodic boundaries. For all the surface results, we simulate systems with 1 x 1 x Z unit cells, where only one unit cell is considered along the in-plane directions (Similar to the quantum calculation by Skomurski *et al.* [30, 31]). The Z-values for (1 0 0), (1 1 0) and (1 1 1) surfaces are calculated based on the convergence of the surface energies. All the surface simulations are performed at 0 K by optimizing the ions in the system, which are predominantly relaxed along the Z-direction. Special care is taken for (1 0 0) and (1 1 1) structures to remove the dipole by moving some of the similar charges from one side to the other before geometrical optimization (check Ref. [31]). The repeat units to build all the surfaces are extracted in such a way that all the angles are  $90^\circ$ . (fractional coordinates of the atoms are listed in Table 9. For (1 0 0) surfaces the repeat unit cell dimensions are  $X = a_0$ ,  $Y = a_0$ , and  $Z = N \times a_0$ , where  $N =$  total number of repeat cells along the Z-direction, and  $a_0 =$   $\text{ThO}_2$  bulk lattice parameter. Each repeat cell contains 4  $\text{ThO}_2$  formula units. For (1 1 0) surfaces the repeat unit cell dimensions are  $X = a_0$ ,  $Y = a_0 / \sqrt{2}$ , and  $Z = N \times (a_0 / \sqrt{2})$ . Each repeat cell contains 2  $\text{ThO}_2$  formula units. For (1 1 1) surfaces the repeat

unit cell dimensions are  $X = a_0 / \sqrt{2}$ ,  $Y = a_0 (\sqrt{3} / \sqrt{2})$ , and  $Z = N \times (\sqrt{3} a_0)$ . Each repeat cell contains 6 ThO<sub>2</sub> formula units. A non-orthogonal repeat cell can also be defined for the (1 1 1) surface repeat cells, which is shown in Ref. [31].

The surface energies are calculated by using the equation:

$$E_{Sur} = \frac{1}{2} [E_{slab} - n \times E_{bulk}] \quad (5)$$

where,  $E_{slab}$  is the energy of the slab,  $E_{bulk}$  is the energy in eV/ThO<sub>2</sub>, and  $n$  is the number of ThO<sub>2</sub> units in the slab. Figures 5, 6 and 7 show the effect of system size on the surface energies for ThO<sub>2</sub> (1 0 0), (1 1 0) and (1 1 1) surfaces respectively. For the (1 0 0) surfaces the converged energy was obtained for a 1 x 1 x 6 unit cells (24 ThO<sub>2</sub> units) with vacuum. Similarly, a size of 1 x 1 x 6 unit cells (12 ThO<sub>2</sub> units) was enough for obtaining convergence for (1 1 0) surfaces, while a supercell of 1 x 1 x 2 unit cells (12 ThO<sub>2</sub> units) was enough for obtaining convergence for (1 1 1) surfaces. Figure 8 compares the energies predicted by each potential to the first-principles calculation results (Table 10). All the potentials predict the (1 1 1) surface to be more favorable (under vacuum condition) for ThO<sub>2</sub>. The general surface energy trend follows (1 1 1) < (1 1 0) < (1 0 0), which is similar to the trend reported for UO<sub>2</sub> [31]. However, under different environment this surface energy stability trend can change. In the presence of adsorbate molecules, Abramowski *et al.* [32] and Tan *et al.* [33] have shown that the more reactive (1 0 0) and (1 1 0) surfaces can be stabilized compared to (1 1 1) in UO<sub>2</sub>. At present, such an investigation is outside the scope of the current article.

In addition to the surface energies, we have analyzed the optimization of atoms near the surface. This is performed by comparing the position of each atom in the fully optimized structures with the respective bulk structures (Table 11). All the atoms at the surface optimize their positions normal to the surface. Figure 9 illustrates the atomic displacements for individual surfaces. It is important to note that the displacements are considered only for atoms which show displacements greater than 0.01 Å.

Considering the (1 1 1) atomic relaxation (Fig. 9a), surface oxygen atoms displace away from the bulk, while near surface Th-atoms displace towards the bulk. Atomic displacements are realized for ~3 atomic layers for (1 1 1) surface. In comparison, only two atomic layers are affected for (1 1 0) surfaces (Fig. 9b), where Th-atoms are displaced more (towards the bulk) compared to the oxygen atoms (away from the bulk).

However, the atomic displacement for (1 0 0) surface appears more complicated. The surface oxygen atoms show displacements towards and away from the bulk (Fig. 9c). A clear picture is illustrated by the three dimensional view representation shown in Fig. 9d. While half of the surface oxygen atoms oriented along the <1 1 0> direction displace towards the bulk, the other half displaces away from the bulk. Similar displacement trend is realized for almost 3 unit cells from the surface. For (1 0 0), the Th-atoms near the surface are displaced away from the bulk. The magnitude of maximum displacement for different surfaces follows (1 1 1) < (1 1 0) < (1 0 0),

which is similar to the maximum displacements reported by Skomurski *et al.* [31] for  $\text{UO}_2$ . NASHK potential shows a different trend in the maximum displacement, which follow  $(1\ 1\ 1) < (1\ 0\ 0) < (1\ 1\ 0)$ .

### 3. Critical Assessment of the Interatomic Potentials

Based on the structure, elastic properties, defect and surface energetic investigated for  $\text{ThO}_2$ , we have summarized the capability and limitations of the nine empirical potentials. This critical assessment is performed by analyzing the capability of each potential to optimize the respective structures, predict the qualitative trend, and predict the quantitative values (wherever applicable) compared to experiment and/or *ab initio* calculations. Our analysis is summarized in Table 12. A tick mark indicates the potential is suitable to investigate the corresponding properties, while a dash represents the potential is not suitable for the listed properties.

Our calculations on the structure, elastic and phonon properties indicate that all the potentials are suitable for investigating bulk properties except NASHK. These 10 potentials all reproduce lattice parameter and moduli satisfactorily.

The relative phase stability for different  $\text{AO}_2$  structures at zero temperature and pressure indicated that the Fluorite is the energetically favorable phase for most of the potentials. However, BD06 is the only potential which resulted in the Cotunnite phase (high temperature, high pressure  $\text{AO}_2$  phase) to be more favorable for  $\text{ThO}_2$ . Even though the Cotunnite phase is predicted to be more favorable, the activation barrier between the Fluorite and Cotunnite phase will be the guiding factor in deciding whether BD06 potential will be suitable to study phase transition in  $\text{ThO}_2$ . Therefore, care must be taken while using BD06 potential for  $\text{ThO}_2$  phase transition.

From the point defect calculations, except BD01 and BD02, all other potentials are able to optimize the structure with defects. However, NASHK potential failed to optimize the structures with defect complexes. Therefore, except NASHK, BD01 and BD02, all other potentials are suitable for investigating  $\text{ThO}_2$  system with defects. Include BD07 discussion here.

All the potentials are suitable for investigating surfaces. In addition to the above assessment, our preliminary work (results not included) shows that NASHK potential resulted in negative phonon frequencies for temperatures  $>800$  K. Therefore, care must be taken while performing high temperature calculations with NASHK potentials. The effect of temperature will provide future confidence in the assessment of these potentials.

As discussed in Section 3.2, BD07 is the only potential which is not suitable to calculate any of the properties investigated in this article. Using different fitting

parameters, new potential interactions for Th-O and/or Th-Th should have to be developed for any future application. Therefore, the present parameter set for BD07 potential should not be used for investigating the properties of ThO<sub>2</sub>.

#### 4. Conclusions

, In this study, we report the successful development of several ThO<sub>2</sub> rigid-ion models suitable for large scale molecular dynamics calculations. The validity of the potentials is evaluated based on the predicted bulk properties. Ground state properties are calculated and compared with experiment and/or first principles computational results. Based on the predicted elastic properties, AO<sub>2</sub> polymorphs, defect energetic and surface stability, a summary of the potentials suitable to investigate the different static properties are provided. High-temperature calculations on bulk ThO<sub>2</sub> will provide further assessment of these potentials and are currently being conducted

#### REFERENCES

- [1] *Thorium Fuel Cycle – Potential Benefits and Challenges*. 2005, International Atomic Energy Agency.
- [2] Govers K, Lemehov S, Hou M and Verwerft M 2007 *Journal of Nuclear Materials* **366** 161-77
- [3] Govers K, Lemehov S, Hou M and Verwerft M 2008 *Journal of Nuclear Materials* **376** 66-77
- [4] Benson G C, Freeman P I and Dempsey E 1963 *Journal of the American Ceramic Society* **46** 43-7
- [5] Mackrodt W C and Stewart R F 1979 *Journal of Physics C-Solid State Physics* **12** 431-49
- [6] Colbourn E A and Mackrodt W C 1983 *Journal of Nuclear Materials* **118** 50-9
- [7] Clausen K, Hayes W, Macdonald J E, Osborn R, Schnabel P G, Hutchings M T and Magerl A 1987 *Journal of the Chemical Society-Faraday Transactions II* **83** 1109-12
- [8] Nadeem M, Akhtar M J, Shaheen R, Haque M N and Khan A Y 2001 *Journal of Materials Science & Technology* **17** 638-42
- [9] Osaka M, Adachi J, Kurosaki K, Uno M and Yamanaka S 2007 *Journal of Nuclear Science and Technology* **44** 1543-9
- [10] *All the potentials are named based on the last initial of all the authors in the articles. For example, the work by Nadeem et al. is referred as NASHK.*
- [11] Tharmalingam K 1971 *Philosophical Magazine* **23** 199-204
- [12] Walker J R and Catlow C R A 1981 *Journal of Physics C-Solid State Physics* **14** L979-L83
- [13] Lewis G V and Catlow C R A 1985 *Journal of Physics C-Solid State Physics* **18** 1149-61
- [14] Sindzingre P and Gillan M J 1988 *Journal of Physics C-Solid State Physics* **21** 4017-31
- [15] Karakasidis T and Lindan P J D 1994 *Journal of Physics-Condensed Matter* **6** 2965-9
- [16] Basak C B, Sengupta A K and Kamath H S 2003 *Journal of Alloys and Compounds* **360** 210-6
- [17] Morelon N D, Ghaleb D, Delaye J M and Van Brutzel L 2003 *Philosophical Magazine* **83** 1533-50
- [18] Arima T, Yamasaki S, Inagaki Y and Idemitsu K 2005 *Journal of Alloys and Compounds* **400** 43-50
- [19] Buckingham R A 1938 *Proceedings of the Royal Society of London Series A-Mathematical and Physical Sciences* **168** 264-83
- [20] Margenau H 1939 *Physical Review* **56** 1000-8

- [21] Morse P M 1929 *Physical Review* **34** 57-64
- [22] Dick B G and Overhauser A W 1958 *Physical Review* **112** 90-103
- [23] Gale J D 1997 *Journal of The Chemical Society, Faraday Transaction* **93** 629-37
- [24] Gale J D and Rohl A L 2003 *Molecular Simulation* **29** 291-341
- [25] Swamy V, Gale J D and Dubrovinsky L S 2001 *Journal of Physics and Chemistry of Solids* **62** 887-95
- [26] Catlow C R A 1977 *Proceedings of the Royal Society of London Series a-Mathematical Physical and Engineering Sciences* **353** 533-61
- [27] Crocombette J P 1999 *Physics and Chemistry of Minerals* **27** 138-43
- [28] Andersson D A, Watanabe T, Deo C and Uberuaga B P 2009 *Physical Review B* **80**
- [29] Willis B T M 1964 *Proceedings of the British Ceramic Society* **1** 9
- [30] Skomurski F N, Shuller L C, Ewing R C and Becker U 2008 *Journal of Nuclear Materials* **375** 290-310
- [31] Skomurski F N, Ewing R C, Rohl A L, Gale J D and Becker U 2006 *American Mineralogist* **91** 1761-72
- [32] Abramowski M, Redfern S E, Grimes R W and Owens S 2001 *Surface Science* **490** 415-20
- [33] Tan A H H, Grimes R W and Owens S 2005 *Journal of Nuclear Materials* **344** 13-6
- [34] Lang S M and Knudsen F P 1956 *Journal of the American Ceramic Society* **39** 415-24
- [35] Macedo P M, Capps W and Wachtman J B 1964 *Journal of the American Ceramic Society* **47** 651-
- [36] Axe J D and Pettit G D 1966 *Physical Review* **151** 676-&
- [37] Yamada K, Kurosaki K, Uno M and Yamanaka S 2000 *Journal of Alloys and Compounds* **307** 10-6

**TABLES****Table 1.** List of articles using interatomic potentials to describe ThO<sub>2</sub> in the literature.

<b>Year published</b>	<b>First author</b>	<b>Properties investigated</b>	<b>Other comments</b>	<b>Referred in this article as</b>
1963	Benson [4]	Lattice parameter, elastic properties, surface energies, compressibility	Partial parameters are listed, not used for this article	Benson <i>et al.</i>
1979	Mackrodt [5]	Lattice parameter, compressibility	Potential parameters not published	Mackrodt <i>et al.</i>
1983	Colbourn [6]	Bulk lattice properties, defects, self-diffusion	Potential parameters not published	Colbourn <i>et al.</i>
1987	Clausen [7]	Phonon dispersion relationship	Potential available but not used for this article	Clausen <i>et al.</i>
2001	Nadeem [8]	Bulk lattice properties, defects, self-diffusion	Potential available and used for current article	NASHK <sup>[10]</sup>
2007	Osaka [9]	Thermal expansion, doping and diffusion	Potential available and used for current article	OAKUY <sup>[10]</sup>

**Table 2.** List of potentials developed in this study to investigate properties of ThO<sub>2</sub>. All these rigid ion models are fitted based on the O-O interactions of the corresponding UO<sub>2</sub> potentials.

Developed models for ThO <sub>2</sub>		Source of O-O interactions from the UO <sub>2</sub> potentials in the literature		
This work [10]	ThO <sub>2</sub> model description	Year published	First author	UO <sub>2</sub> model description
BD01	Buckingham with D-term	1971	Tharmalingam [11]	Buckingham
BD02	Buckingham with D-term	1971	Tharmalingam [11]	Buckingham with D-term
BD03	Buckingham	1981	Walker [12]	Buckingham
BD04	Buckingham	1985	Lewis [13]	Buckingham
BD05	Buckingham-4	1988	Sindzingre* [14]	Buckingham-4
		1994	Karakasidis* [15]	
BD06	Buckingham + Morse	2003	Basak [16]	Buckingham + Morse
BD07		2003	Morelon [17]	Buckingham-4
BD08	Buckingham	2005	Arima [18]	Buckingham
BD09	Buckingham	2005	Arima [18]	Buckingham

\* These UO<sub>2</sub> potentials have same O-O interactions with same charges. The ThO<sub>2</sub> potential based on this O-O interaction will be the same. However, for ThO<sub>2</sub>-UO<sub>2</sub> mixed systems, these will be regarded as two different sets of potentials. For future references, a UO<sub>2</sub>-ThO<sub>2</sub> mixed system with Sindzingre UO<sub>2</sub> description should be referred as BD05S, and with Karakasidis description as BD05K.

**Table 3.** Potential parameters for ThO<sub>2</sub> interatomic interactions

Potential Details	Nadeem	Osaka	Tharmalingam1	Tharmalingam2	Walker	Lewis	Karakasidis <sup>†</sup>	Basak	Morello <sup>†</sup>	Arima1	Arima2
Referred as	NASHK	OAKUY	BD01	BD02	BD03	BD04	BD05	BD06	BD07	BD08	BD09
<b>q [e] (Charge)</b>											
Th_core	4.64	2.4	4.0	4.0	4.0	4.0	4.0	2.4	3.2272	4.0	2.7
Th_shel	-0.64								52		
O_Core	0.513	-1.2	-2.0	-2.0	-2.0	-2.0	-2.0	-1.2	-	-2.0	-1.35
O_shel	-2.513								1.6136		
<b>k<sub>2</sub> [eV·Å<sup>-2</sup>] (Spring)</b>									26		
Th	110										
O	20.53										
<b>O-O (Buckingham)</b>											
A [eV]	25.41	2346.14	-93.3	36.1	50259.	22764	11272.6	1633.666	11272.	22517.	919.17
ρ [Å]	0.6937	88	0.398	0.382	34	.3	0.1363	6	6	53	0.332
C [eV·Å <sup>6</sup> ]	32.32	17.3393	0	16.85	0.1528	0.149	134	3.95063	0.1363	0.149	17.36
D [eV·Å <sup>8</sup> ]		6		11.86	5	112.2			134	27.59	
<b>Th-O (Buckingham)</b>											
A [eV]	8638.5	61.4295	2207.565	1896.302	1379.8	1978.	1042.528	1081.000	607.11	1594.9	27166.
					66	75		4	4	96	11

$\rho$ [Å]	0.2856	0.57	0.369615	0.37396	0.3986 73	0.387 74 244.9	0.408121	0.33059	0.4081 2	0.3939 55	0.2248 57
C [eV·Å <sup>6</sup> ]	70		36.715	0.31	49.22	41	0			73.96	12.8
D [eV·Å <sup>8</sup> ]			257.96	42.63							
<b>Th-Th (Buckingham)</b>											
A [eV]		17.0261	0	0	8.5215 0.1666			11464.05 07		9.815 0.3150	
$\rho$ [Å]		0.82	0.398	0.382	6 1530.1			0.15984		62 2593.1	
C [eV·Å <sup>6</sup> ]			170	244.18	73					18	
D [eV·Å <sup>8</sup> ]			20370.45	31974.16							
<b>Th-O (Morse)</b>											
D [eV]		1.215						1.00879	0.6268 02		
$\beta_{ij}$ [1/Å]		1.9						1.60473	0.0927 58		
$r^*_{ij}$ [Å]		2.36						2.369	9.2188 93		

† Spline parameters for Karakasidis and Morelon models are  $r_1 = 1.2$  Å,  $r_{\min} = 2.1$  Å,  $r_2 = 2.6$  Å

**Table 4.** Comparison of bulk properties of ThO<sub>2</sub> calculated from different interatomic potentials with experiment

	Experiment	NASH K	OAKU Y	BD01	BD02	BD03	BD04	BD05	BD06	BD07	BD08	BD09
Lattice parameter [Å]	5.5997 [34]	5.5946	5.5797	5.599 9	5.599 9	5.600 0	5.599 5	5.600 0	5.599 5	5.600 0	5.599 8	5.600 1
Volume [Å <sup>3</sup> ]	175.59	175.11	173.71	175.6 0	175.6 1	175.6 1	175.5 7	175.6 1	175.5 7	175.5 7	175.6 0	175.6 3
Lattice Energy (eV/ThO <sub>2</sub> )												
C <sub>11</sub> [GPa]	367 [35]	573	441	366	367	367	367	368	367	368	366	367
C <sub>12</sub> [GPa]	106 [35]	168	93	106	106	106	106	106	106	106	106	106
C <sub>44</sub> [GPa]	79 [35]	132	86	99	89	103	105	104	82	89	97	95
Bulk Mod. [GPa]	198	303	209	193	193	193	193	193	193	193	193	193
Shear Mod [GPa]	100, 103 [4]	157	115	111	104	113	115	114	99	104	109	108
Young's Mod [GPa]	256, 270 [4]	496	408	319	320	319	320	320	319	320	319	320
Poisson's ration	0.279	0.227	0.175	0.224	0.224	0.224	0.224	0.223	0.224	0.223	0.224	0.224
Compressibility [10 <sup>-3</sup> /GPa]	4.16 [4]			5.19	5.18	5.19	5.19	5.18	5.18	5.18	5.19	5.18
Static Dielec. Const.	18.9 [36]	18.95	2.82	6.16	5.21	7.19	9.47	9.67	2.60	13.33	6.16	3.26
High. Freq. Di Const.	4.3, 4.86 [36]	4.42										
Phonons at $\Gamma$ (293 K)												
T. mode (cm <sup>-1</sup> )	269.2 [7]	220.3	347.5	348.4	385.1	317.5	272.1	267.1	373.5	180.0	385.1	348.4
L. mode (cm <sup>-1</sup> )	569.8 [7]	418.6	592.1	517.0	559.7	485.9	436.0	418.9	580.1	276.7	559.7	522.7

**Table 5.** Relative energies of different AB<sub>2</sub> polymorphs of ThO<sub>2</sub> with respect to the Fluorite structure calculated from different interatomic potentials (in eV/ThO<sub>2</sub>).

Phases	NASHK	OAKUY	BD01	BD02	BD03	BD04	BD05	BD06*	BD08	BD09
Anatase	0.48	0.49	1.26	1.38	1.19	0.91	0.45	1.74	1.60	0.57
Baddeleyite	-	0.20	0.59	f	f	f	f	0.31	f	f
Brookite	-	0.40	0.57	0.38	f	f	f	0.28	f	0.54
Columbite	-	0.26	f	f	f	f	f	f	f	0.42
Cotunnite	-	0.41	0.26	-	0.46	0.68	0.87	<b>-0.23</b>	0.12	0.53
Hollandite	-	0.72	1.69	1.77	1.74	1.54	1.02	1.90	2.10	0.86
Pyrite	f	0.26	f	f	f	f	f	f	f	f
Ramsdellite	f	f	f	-	f	f	f	f	f	f
Rutile	0.57	0.23	0.91	1.01	0.76	0.59	0.38	1.07	1.00	0.40
TiO <sub>2</sub> B	-	0.69	1.52	-	1.43	1.08	0.73	1.76	-	0.81

Note: Blank data spaces indicate that optimization of the structures with the potentials were not achieved.

f – indicates the structures optimized to the Fluorite structure

\* - indicates potential predicting phase other than the Fluorite phase to be energetically more stable

The data in bold represents the most stable structure predicted with the potentials.

**Table 6.** Relative energies of different AB<sub>2</sub> polymorphs of UO<sub>2</sub> with respect to the Fluorite structure calculated from different interatomic potentials (in eV/UO<sub>2</sub>).

Phases	Nadeem* [8]	Osaka [37]	Tharmaling am1 [11]	Tharmaling am2 [11]	Walker [12]	Lewis* [13]	Sindzinger	Karakasidis [15]	Basak [16]	Morelone* [17]	Arima1 [18]	Arima2* [18]
Anatase	0.53	1.15	<b>-0.21</b>	-0.04	<b>-0.13</b>	0.44	-0.12	<b>-0.05</b>	0.49	0.39	-0.03	0.44
Baddeleyite		f	-0.10	-0.09	-0.04	f	-0.05	f	0.06	f	-0.01	f
Brookite		<b>-0.23</b>	f	0.07	0.07	f	0.07	0.12	0.28	f	0.13	0.43
Columbite		f	-0.10	-0.09	-0.04	f	-0.05	f	0.04	f	-0.01	0.32
Cotunnite		<b>-0.23</b>	-0.17	0.90	f	0.90	<b>-0.14</b>	-0.01	0.19	0.53	0.96	0.61
Hollandite		0.65	0.40	0.60	0.52	1.03	0.51	0.58	0.74	0.75	0.59	0.75
Pyrite	f	-0.14	0.03	0.02	f	f	f	f	<b>0.02</b>	f	f	f
Ramsdellite		0.04	0.40	f	f	f	-0.01	f	f	f	f	0.74
Rutile	0.63	0.28	-0.14	<b>-0.11</b>	-0.07	0.37	-0.04	f	0.05	0.36	<b>-0.04</b>	0.29
TiO <sub>2</sub> B		1.31	-0.03		0.13	0.72	-0.03	0.06	0.62	0.61	-0.03	0.71

Note: Blank data spaces indicate that optimization of the structures with the potentials were not achieved.

f – indicates the structures optimized to the Fluorite structure

\* - indicates the potentials predicting Fluorite to be the most stable structure

The data in bold represents the most stable structure predicted with the potentials.

**Table 7.** Comparison of formation energies of simple and complex defects in ThO<sub>2</sub> calculated from different interatomic potentials with published values

Defects	REF [8]	REF [6]	NASHK	OAK UY	BD01	BD02	BD03	BD04	BD05	BD06	BD08	BD09
<b>Point defects [eV]</b>												
O Interstitial (O <sub>i</sub> )		-9.82	-6.82	0.17	-4.92	-2.49	-7.58	-10.54	-9.98	-1.73	-5.89	-1.29
O Vacancy (V <sub>O</sub> )	13.94	15.83	13.42	7.47	15.72		14.99	17.01	16.52	8.88	13.82	8.65
Th Interstitial (Th <sub>i</sub> )		-64.86	-69.13	-21.34	-64.46		-56.07	-56.07	-54.41	-24.31	-69.14	-24.70
Th Vacancy (V <sub>Th</sub> )	89.07	84.66	88.51	41.91	89.95	94.42	81.42	81.42	78.92	46.09	93.77	46.93
<b>Defect Complexes [eV]</b>												
<b>Frenkel Pairs</b>												
OFP <sub>∞</sub> (V <sub>O</sub> + O <sub>i</sub> )		6.01	6.60	7.64	10.80		7.41	6.47	6.53	7.15	7.93	7.36
OFP <sub>1</sub>				6.83		6.78	6.17	5.37	5.45	6.25	6.58	6.40
OFP <sub>2</sub>				6.32	6.74		5.90	5.23	5.30	5.86	6.24	5.94
ThFP <sub>∞</sub> (V <sub>Th</sub> + Th <sub>i</sub> )		19.80	19.39	20.56	25.49		25.22	25.35	24.51	21.78	24.62	22.23
ThFP <sub>1</sub>				15.56	15.19		21.23	20.10	19.29	16.47	18.02	16.67
<b>Schottky</b>												
Sch <sub>∞</sub> (V <sub>Th</sub> + 2 V <sub>O</sub> )	11.98	11.93	10.39	13.79	20.53		17.43	14.08	12.16	18.94	20.66	14.62
Sch <sub>1</sub>			5.41	6.05	11.92	12.08	9.13	7.72	6.09	9.62	10.85	6.23
Sch <sub>2</sub>			5.40	6.35		12.20	9.37	7.87	6.24	9.92	11.14	6.53
Sch <sub>3</sub>				7.38	13.00	13.63	10.52	8.73	7.07	11.02	12.49	7.63

**Table 8.** Comparison of binding energies of charged complex defect clusters in ThO<sub>2</sub> calculated from different interatomic potentials with published values

Defects	REF [8]	REF [6]	NASHK	OAK UY	BD01	BD02	BD03	BD04	BD05	BD06	BD08	BD09
<b>Binding Energies [eV]</b>												
<b>Diinterstitials</b>												
Dii <sub>m</sub> (Th <sub>i</sub> + O <sub>i</sub> )				3.38			3.62	2.91	2.97	3.43		3.64
Dii <sub>O</sub> (O <sub>i</sub> + O <sub>i</sub> )				-1.53	2.62	2.66	-1.63	-1.24	-1.14	-1.69	-1.94	-1.58
Dii <sub>Th</sub> (Th <sub>i</sub> + Th <sub>i</sub> )				-6.12	-1.95			-6.04	-6.04	-6.45		-6.64
<b>Divacancies</b>												
Div <sub>m</sub> (V <sub>Th</sub> + V <sub>O</sub> )		2.74		4.34	6.04		4.59	3.50	3.34	5.17	5.42	4.70
Div <sub>O1</sub> (V <sub>O</sub> + V <sub>O</sub> )				-1.64	-1.94		-1.73	-1.28	-1.30	-1.70	-2.01	-1.78
Div <sub>O2</sub> (V <sub>O</sub> + V <sub>O</sub> )				-1.78	-2.46		-1.92	-1.47	-1.44	-1.93	-2.25	-1.87
Div <sub>O3</sub> (V <sub>O</sub> + V <sub>O</sub> )				-2.89	-3.02		-3.13	-2.53	-2.42	-3.04	-3.58	-2.88
Div <sub>Th</sub> (V <sub>Th</sub> + V <sub>Th</sub> )				-7.51	-9.78		-7.98	-5.74	-6.15	-7.70	-9.14	-8.09
<b>Tetravacancy</b>												
Tetrav <sub>m</sub> (2 V <sub>Th</sub> + 2 V <sub>O</sub> )				8.74			5.41	9.15	6.63	11.17	11.41	9.46

**Table 9.** Fractional coordinates of orthogonal unit cells repeated to generate (100), (110) and (111) surfaces.  $a_0$  represents the bulk ThO<sub>2</sub> lattice parameter.

(100) <sup>†</sup>				(110)				(111) <sup>†</sup>			
	$a_0$	$a_0$	$a_0$		$a_0$	$a_0/\sqrt{2}$	$a_0/\sqrt{2}$		$a_0/\sqrt{2}$	$(\sqrt{3}/\sqrt{2})a_0$	$\sqrt{3}a_0$
Th	0.00000	0.00000	0.00000	Th	0.00000	0.00000	0.00000	Th	0.00000	0.00000	0.00000
Th	0.50000	0.50000	0.00000	Th	0.50000	0.50000	0.50000	Th	0.50000	0.50000	0.00000
Th	0.50000	0.00000	0.50000	O	0.25000	0.50000	0.00000	Th	0.50000	0.16667	0.33333
Th	0.00000	0.50000	0.50000	O	0.75000	0.50000	0.00000	Th	0.00000	0.66667	0.33333
O	0.25000	0.25000	0.25000	O	0.25000	0.00000	0.50000	Th	0.00000	0.33333	0.66667
O	0.25000	0.25000	0.75000	O	0.75000	0.00000	0.50000	Th	0.50000	0.83333	0.66667
O	0.25000	0.75000	0.25000					O	0.00000	0.00000	0.25000
O	0.75000	0.25000	0.25000					O	0.00000	0.00000	0.75000
O	0.75000	0.75000	0.25000					O	0.50000	0.50000	0.25000
O	0.75000	0.25000	0.75000					O	0.50000	0.50000	0.75000
O	0.25000	0.75000	0.75000					O	0.50000	0.16667	0.08333
O	0.75000	0.75000	0.75000					O	0.50000	0.16667	0.58333
								O	0.00000	0.66667	0.08333
								O	0.00000	0.66667	0.58333
								O	0.00000	0.33333	0.41667
								O	0.00000	0.33333	0.91667
								O	0.50000	0.83333	0.41667
								O	0.50000	0.83333	0.91667

<sup>†</sup> – Surface oxygen atoms should be rearranged to cancel the dipole created for (100) and (111) polar surfaces

**Table 10.** Comparison of optimized low-index surface energies of ThO<sub>2</sub> calculated from different interatomic potentials

Surface energies (J/m <sup>2</sup> )	DFT [30]	NASHK	OAKUY	BD01	BD02	BD03	BD04	BD05	BD06	BD08	BD09
(100)	1.75	2.94	2.25	3.50	3.82	3.45	2.98	2.44	3.33	4.03	2.22
(110)	1.30	1.43	1.71	2.76	2.91	2.91	2.68	2.14	2.58	3.37	1.63
(111)	0.72	0.90	1.05	1.72	1.83	1.91	1.75	1.28	1.83	2.27	0.98

**Table 11.** Maximum displacement of atoms at the surface layer of ThO<sub>2</sub> calculated from different interatomic potentials. The results are compared with maximum surface relaxation for UO<sub>2</sub> surfaces calculated with first-principles calculations [31].

	DFT (UO <sub>2</sub> )	NASHK <sup>†</sup>	OAKUY	BD01	BD02	BD03	BD04	BD05	BD06	BD08	BD09
(1 0 0)	0.33	0.30	0.28	0.42	0.37	0.42	0.50	0.50	0.25	0.37	0.31
(1 1 0) *	0.18	0.35	0.13	0.16	0.16	0.14	0.15	0.16	0.11	0.14	0.12
(1 1 1)	0.02	0.08	0.02	0.03	<0.01	0.04	0.09	0.12	0.06	0.02	0.01

Note: For NASHK the relative displacement order is (1 1 1) < (1 0 0) < (1 1 0)

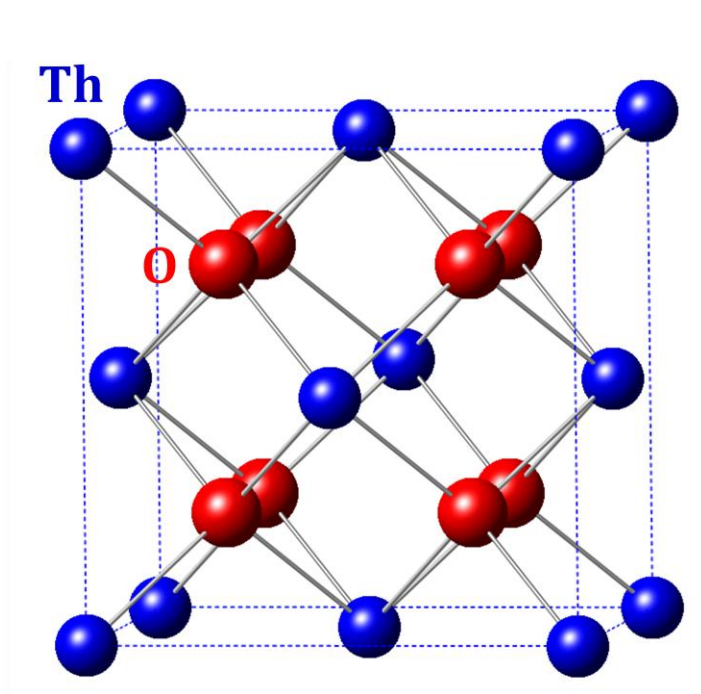
<sup>†</sup> – Average core-shell displacement

\* - The maximum displacement corresponds to Th-atoms

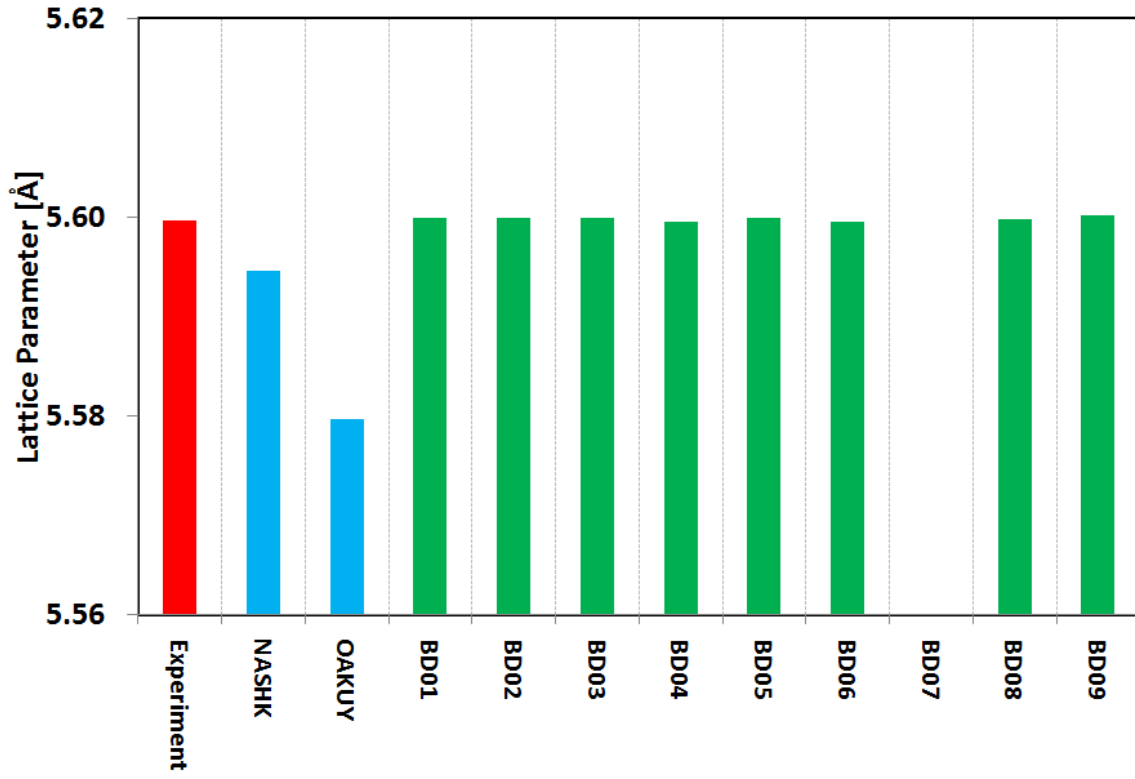
**Table 12.** Assessment of all the interatomic potentials to investigate static properties of ThO<sub>2</sub>

Properties	NASHK	OAKUY	BD01	BD02	BD03	BD04	BD05	BD06	BD07	BD08	BD09
Elastic Properties	-	✓	✓	✓	✓	✓	✓	✓	✓	✓	✓
Phase Stability	✓	✓	✓	✓	✓	✓	✓	-	-	✓	✓
Point Defects	✓	✓	-	-	✓	✓	✓	✓	-	✓	✓
Defect Complexes	-	✓	-	-	✓	✓	✓	✓	-	✓	✓
Surface Stability	✓	✓	✓	✓	✓	✓	✓	✓	-	✓	✓

Note: Places without a tick mark indicates the potential is not suitable to investigate the properties of interest.

**FIGURES**

**Fig. 1.** Schematic of a ThO<sub>2</sub> unit cell.



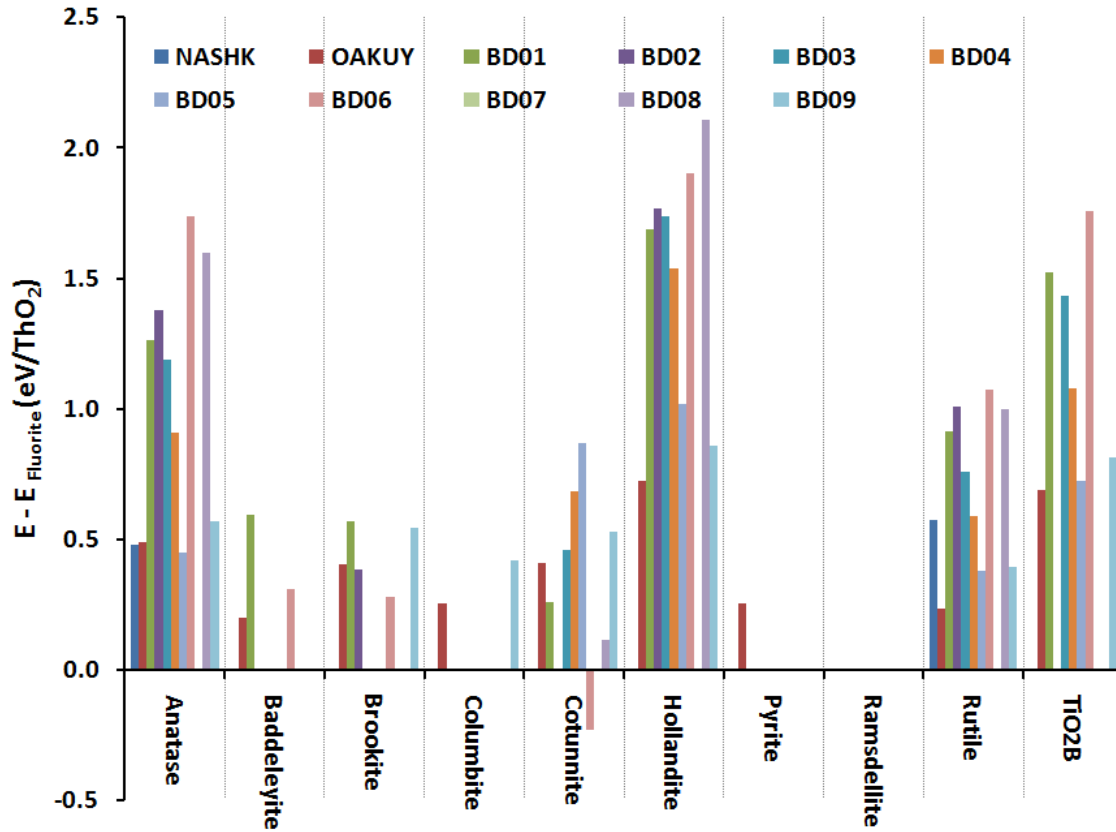


**Fig. 2.** Energy of different AB<sub>2</sub> polymorphs compared with the Fluorite structure for ThO<sub>2</sub> (in eV/ThO<sub>2</sub>) using different interatomic potentials.

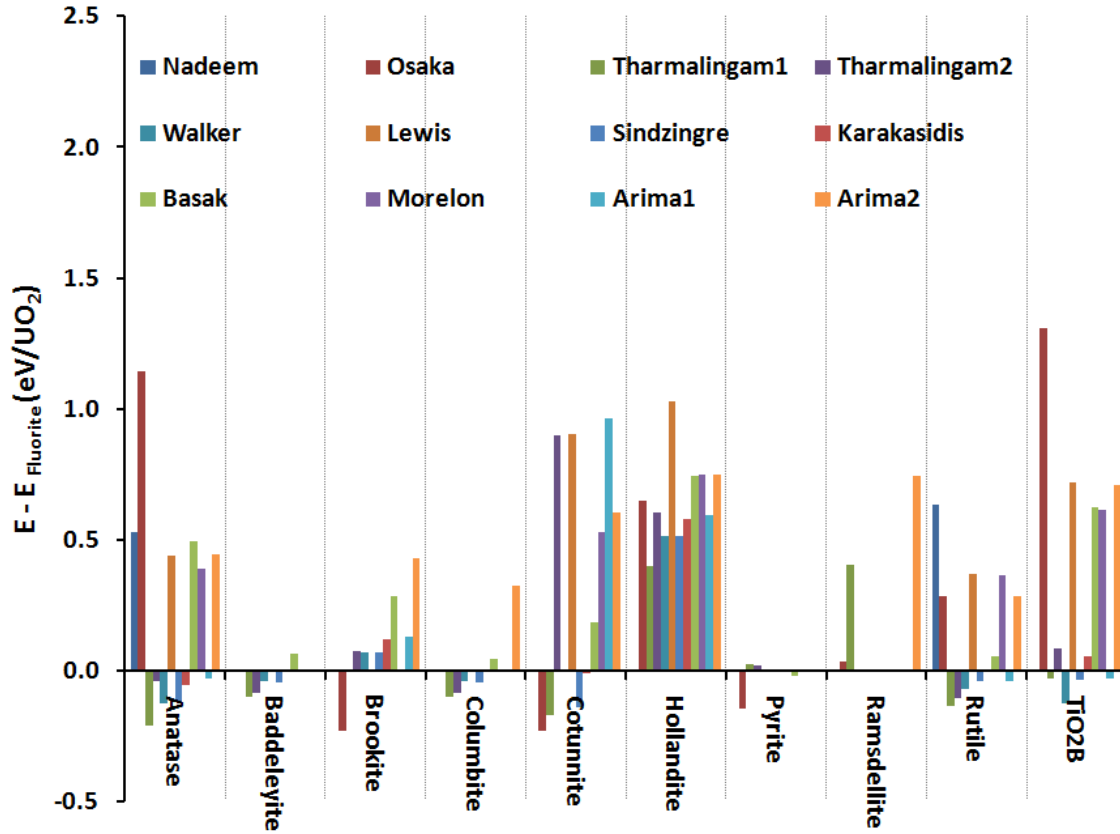


**Fig. 3.** Energy of different  $AB_2$  polymorphs compared with the Fluorite structure for  $UO_2$  (in  $eV/UO_2$ ) using different interatomic potentials.

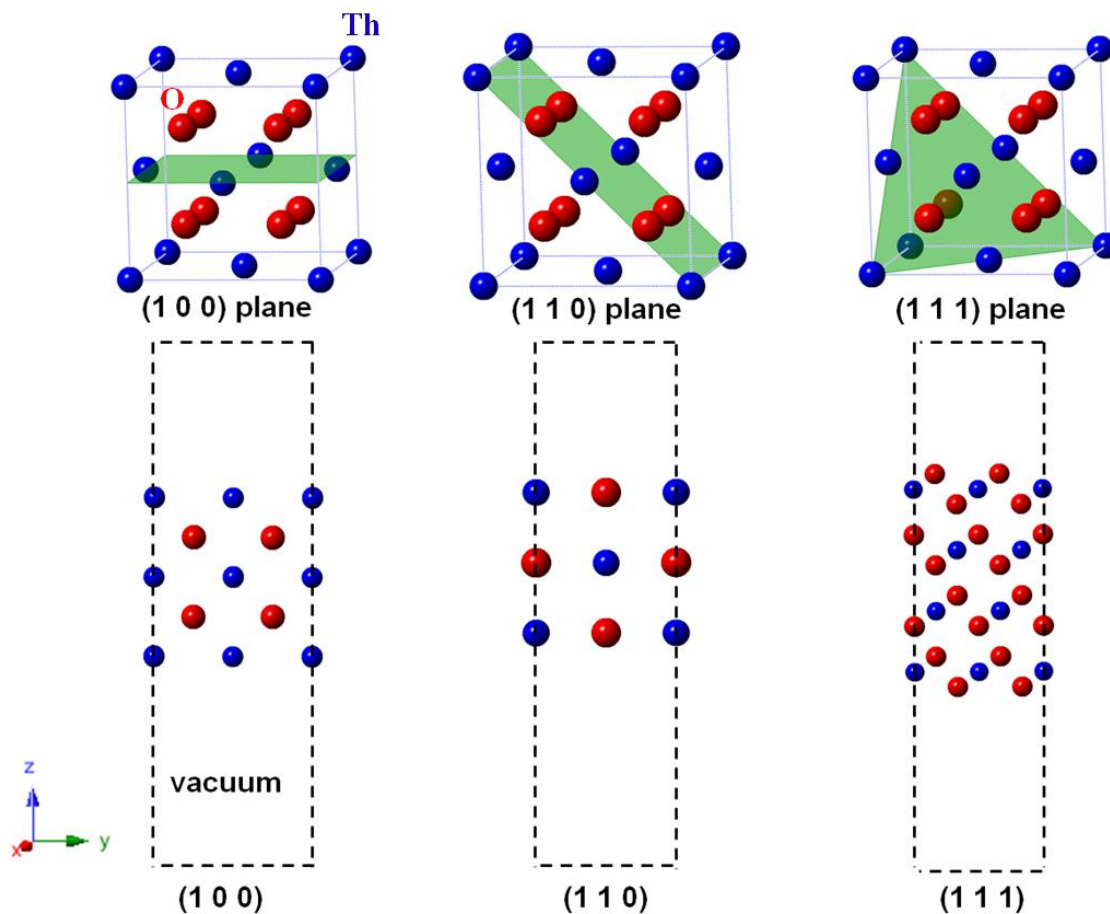


**Fig. 4.** Schematic of (1 0 0), (1 1 0), and (1 1 1) surface cells used to estimate surface energies. The top figures illustrate the respective planes in a bulk ThO<sub>2</sub> unit cell. A vacuum of 30 Å is added along the Z-direction to generate the surface. The (1 0 0) surface shows a Th/O/Th/O... layering sequence, the (1 1 0) surface has both Th and O in each layer, while for (1 1 1) surface structure the definition of layer is not as obvious. However, a repeat layer of Th/O/Th or O/Th/O can be defined for the (1 1 1) surface.

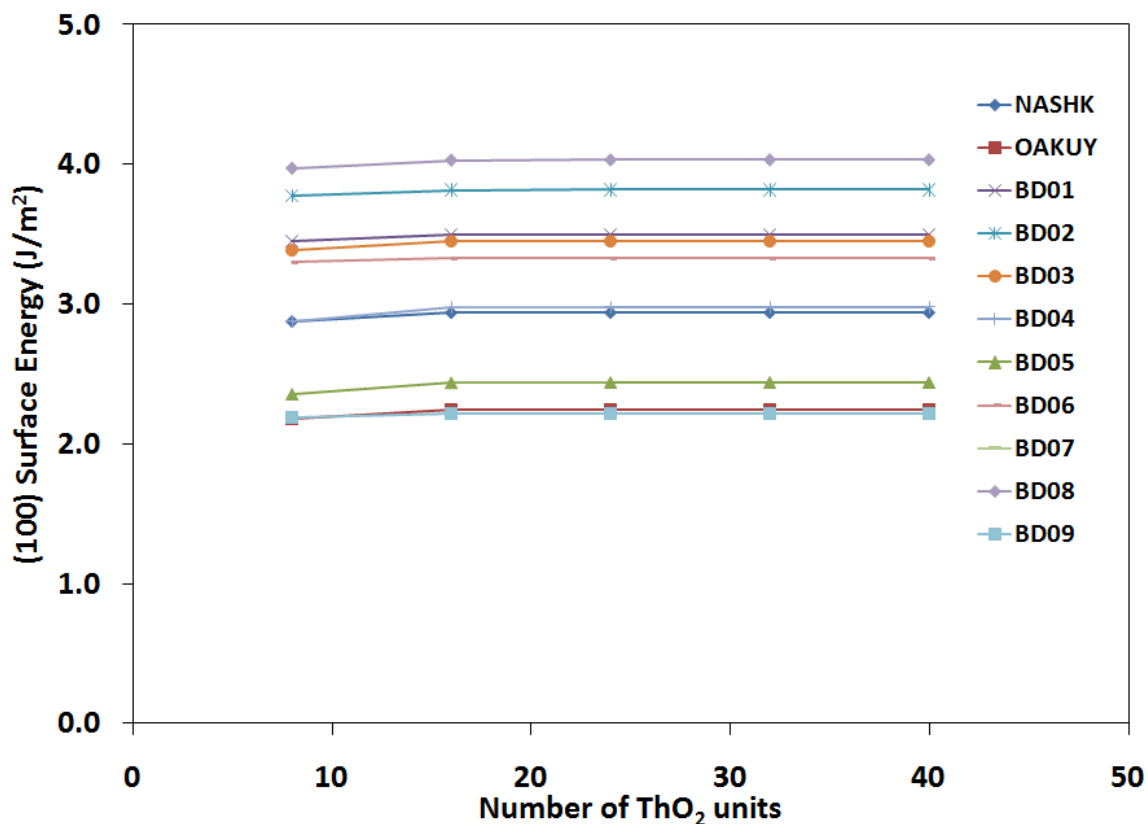


**Fig. 5.** Convergence test for (1 0 0) surface energies of ThO<sub>2</sub> calculated by analyzing the effect of system size for a 1 x 1 x Z structure, where Z is the number of unit cells perpendicular to the surface. One unit cell of ThO<sub>2</sub> contained 4 ThO<sub>2</sub> units. The (1 0 0) surfaces were not stable for Arima1, Tharmalingam1 and Walker potentials.

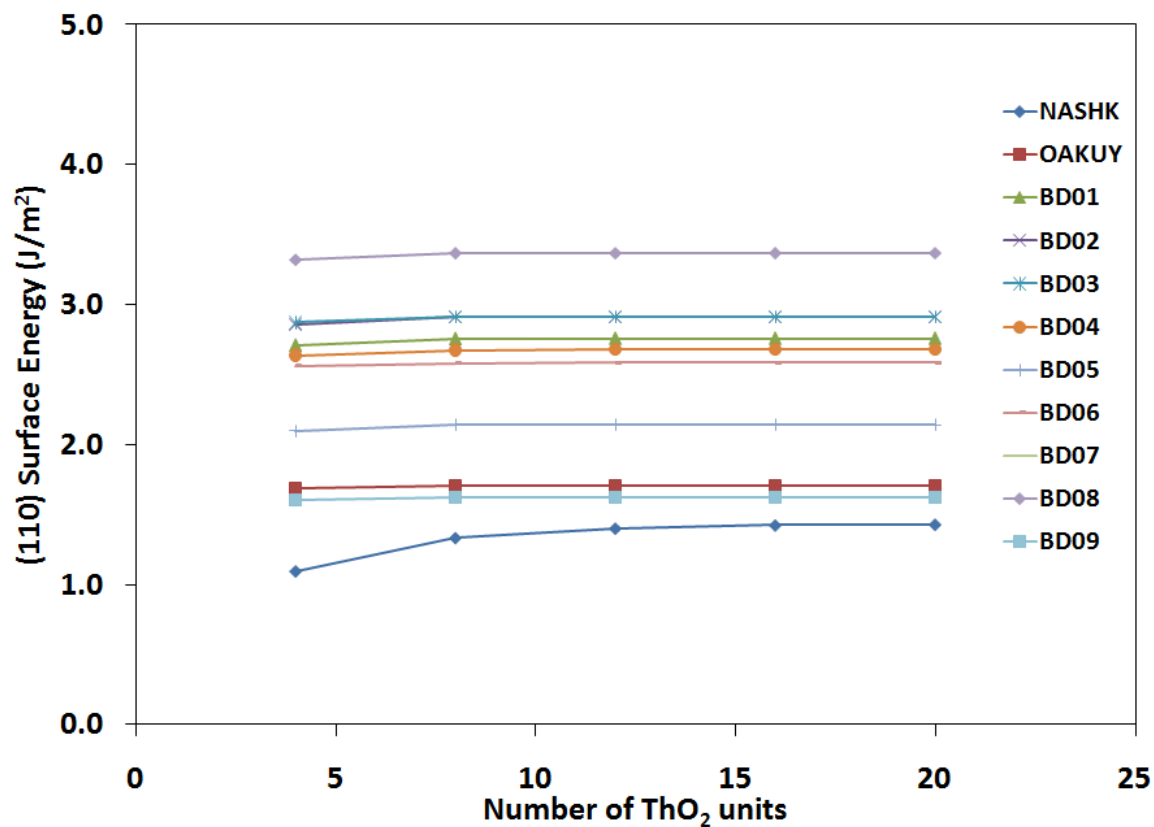


**Fig. 6.** Convergence test for (1 1 0) surface energies of ThO<sub>2</sub> calculated by analyzing the effect of system size for a 1 x 1 x Z structure, where Z is the number of unit cells perpendicular to the surface. One unit cell of ThO<sub>2</sub> contained 2 ThO<sub>2</sub> units.

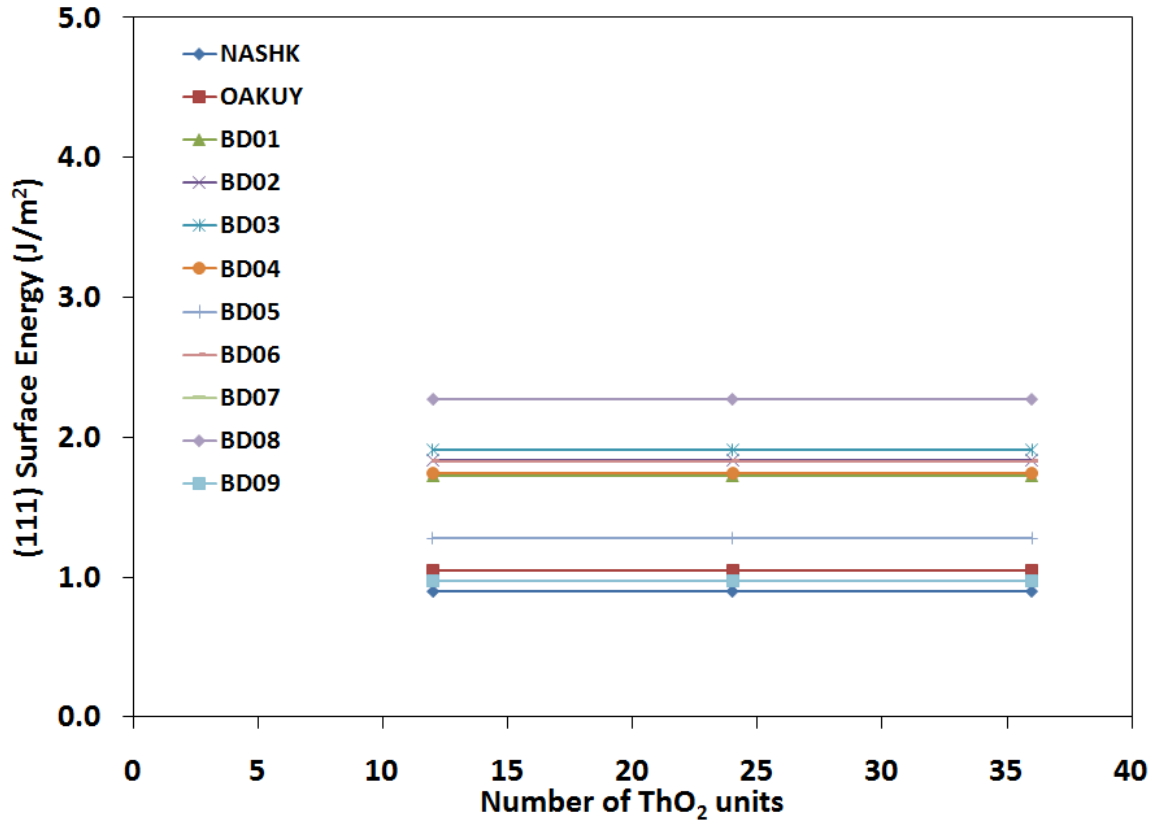


**Fig. 7.** Convergence test for (1 1 1) surface energies of ThO<sub>2</sub> calculated by analyzing the effect of system size for a 1 x 1 x Z structure, where Z is the number of unit cells perpendicular to the surface. One unit cell of ThO<sub>2</sub> contained 6 ThO<sub>2</sub> units.

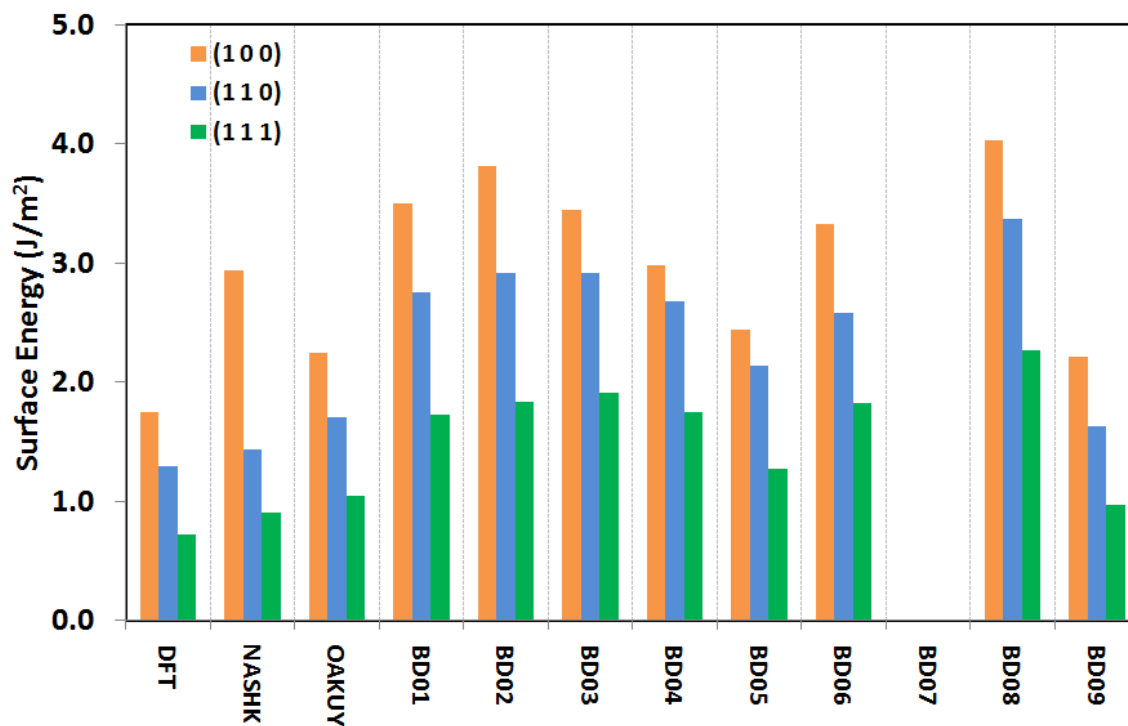


**Fig. 8.** Surface energies of low-index  $\text{ThO}_2$  surfaces calculated from different interatomic potentials. (1 1 1) is predicted to be the most favorable surface with all the potentials. The (1 0 0) surfaces were not stable for Arima1, Tharmalingam1 and Walker potentials.

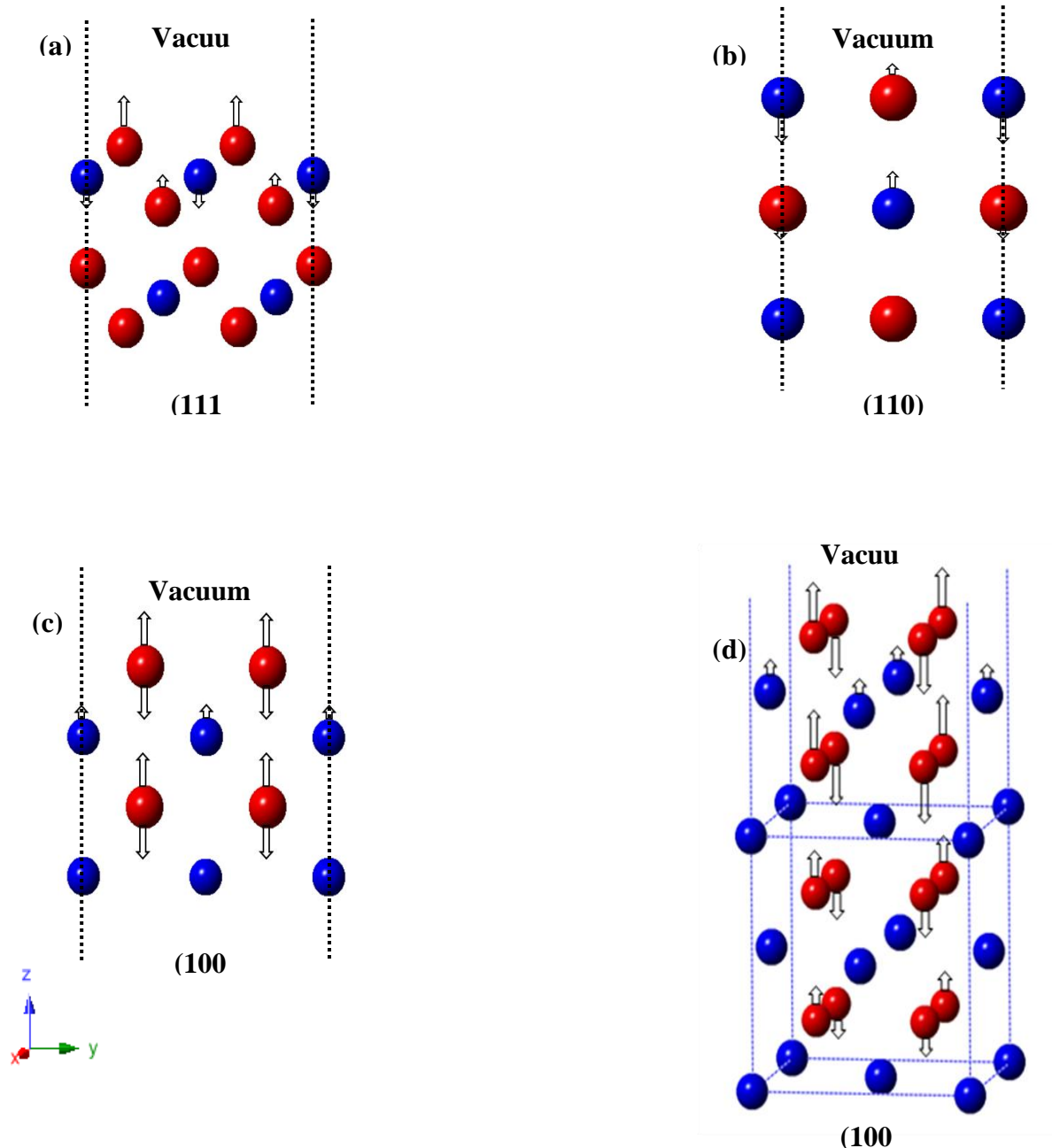


**Fig. 9.** Illustration of atomic displacements (side view) observed in (a) (1 1 1), (b) (1 1 0), and (c) (1 0 0) ThO<sub>2</sub> surfaces. Oxygen atoms at the (1 1 1) and (1 1 0) surfaces optimize away from the bulk, while Th-atoms relax towards the bulk. For (1 0 0) surfaces the atomic displacement is a bit complicated, where half of the surface oxygen atoms relax towards the bulk (along  $\langle 1\ 1\ 0 \rangle$ ) and the other half relax away from the bulk. This trend continues for almost 3 unit cells from the surface. This displacement pattern is represented by the 3D figure shown in (d). In each figure, the arrows indicate the direction of atomic displacement relative to the bulk position.